`

Numerical modelling of Tsunami Effects at Port Waikato, Raglan and Aotea
Waikato West Coast, New Zealand

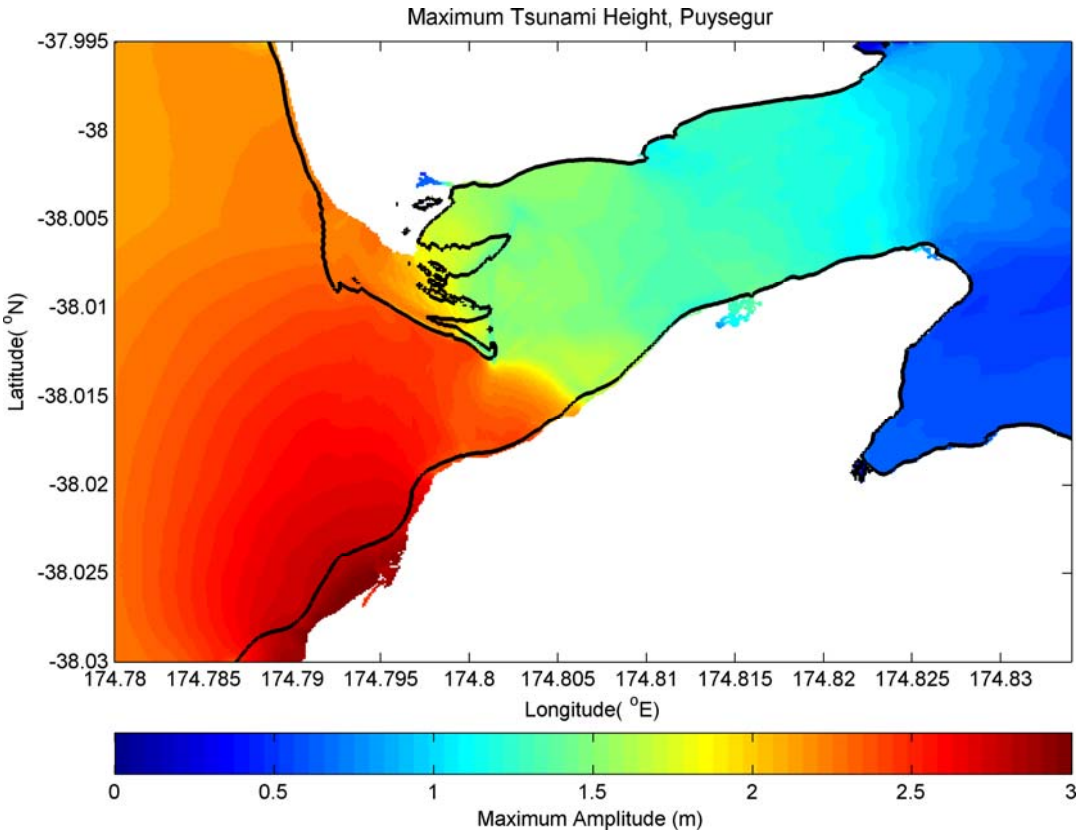

eCoast Limited
Marine Consulting and Research
P.O. Box 151
Raglan, New Zealand

jose@ecoast.co.nz

Numerical modelling of Tsunami Effects at Port Waikato, Raglan and Aotea Waikato West Coast, New Zealand

Report Status

Version	Date	Status	Approved By:
V 1	13 October 2015	DRAFT	JCB/SMO
V 2	4 December 2015	FINAL	JCB/RL
V 2	3 February 2016	FINAL – R1	JCB

It is the responsibility of the reader to verify the currency of the version number of this report.

Jose C. Borrero Ph.D.
Sam O'Neill M.Sc.

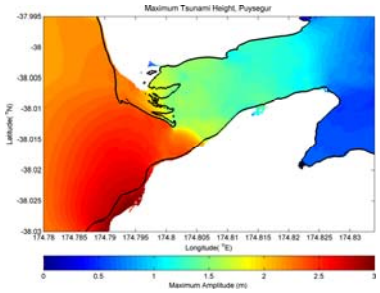

Cover Picture: Maximum tsunami heights at the entrance to Aotea Harbour generated by an earthquake on the Puysegur Trench

TABLE OF CONTENTS

TABLE OF FIGURES

TABLE OF TABLES

1 INTRODUCTION

This report describes the assessment of tsunami effects resulting from regional and distant tectonic (earthquake) sources at Port Waikato, Raglan (Whaingaroa) Harbour and Aotea Harbour located on the west coast of New Zealand's North Island (Figure 1.1). These effects include the quantification of maximum and minimum tsunami wave heights, the extents of tsunami inundation and tsunami induced current speeds. The results from this study are intended to guide emergency management and evacuation planning activities. As such, this study focuses primarily on extreme tsunami scenarios in an effort to define likely maximum credible events for the purposes of planning evacuation routes and increasing public awareness. This report extends tsunami inundation and hazard studies previously completed by Borrero (2013, 2014). This study also carries on from the works of Power *et al.* (2011) and Goff and Chagué-Goff (2015). The former analysed the tsunami hazards posed to New Zealand from the Tonga-Kermadec and Southern New Hebrides subduction margins, while the latter reviewed the history of tsunamis on the west coast of New Zealand over the past 700 years.

1.1 Definition of Tsunami Source Regions

Tsunami sources are generally grouped according to the tsunami wave travel time from the source region to the site of interest. For the New Zealand context, Power (2013) groped sources according to the following definitions:

- Distant source – more than 3 hours travel time from New Zealand
- Regional source – 1–3 hours travel time from New Zealand
- Local source – 0–60 minutes travel time to the nearest New Zealand coast

This study focuses on tsunamis generated by sources located in the Solomon Islands and along the Southern New Hebrides, Tonga-Kermadec and Puysegur Trenches (see Figure 1.2). Strictly speaking, based on these definitions and the computed travel times (presented in Section 3) for the west coast of the Waikato, the Southern New Hebrides, Tonga-Kermadec and Puysegur trench sources would be considered 'regional' while the Solomon Island sources would be considered 'distant source'. However, considering the geography of the southwest Pacific and when comparing arrival times in New Zealand for tsunamis coming from South America (arrivals in 14-17 hours, see Section 4), it is advantageous to consider tsunamis emanating from the Solomon Islands sources as 'regional' and to cluster these events with the other source regions located in the southwest Pacific.

For the regional/distant source events located in the south western Pacific, we consider a large magnitude (M9.0) event located along each subduction zone plate boundary, constructed with uniform slip distribution. For the Solomon and Tonga-Kermadec Trenches, two separate cases are considered, accounting for portions with differing strike orientations along the former, and to observe the differing effects associated with shifting the source region along the latter (see Figure 2.1).

For the distant source events, we consider only South American tsunamis for two reasons; firstly, sensitivity studies for Pacific Rim tsunamis conducted by Borrero et al. (2014) suggest that for a given earthquake size, tsunamis originating from South

America have a larger impact in New Zealand than do tsunamis originating form most other parts of the Pacific Rim, and secondly, the South American Subduction Zone (SASZ) has a well-known history of producing very large earthquakes (>M8.5) and is likely to produce another such event in coming decades. While the sensitivity study of Borrero et al. (2014) show that tsunamis originating from Central America produce somewhat larger tsunami heights in New Zealand than a South American source of equivalent magnitude, the subduction zone offshore of Central America has never produced an earthquake with sufficient magnitude to generate a trans-pacific tsunami. For this reason, tsunamis from Central America are not considered here, nor are large magnitude events from other parts of the Pacific Rim. Given the historical record and the results from Borrero *et al.* (2014) we assume that the cases modelled here represent the maximum credible far-field events.

We use the current state-of-the art tsunami modelling tools (ComMIT: Titov et al. 2011) and the most recent scientific literature on the relevant tsunami source mechanisms. Model results are compared quantitatively and qualitatively to available historical information.

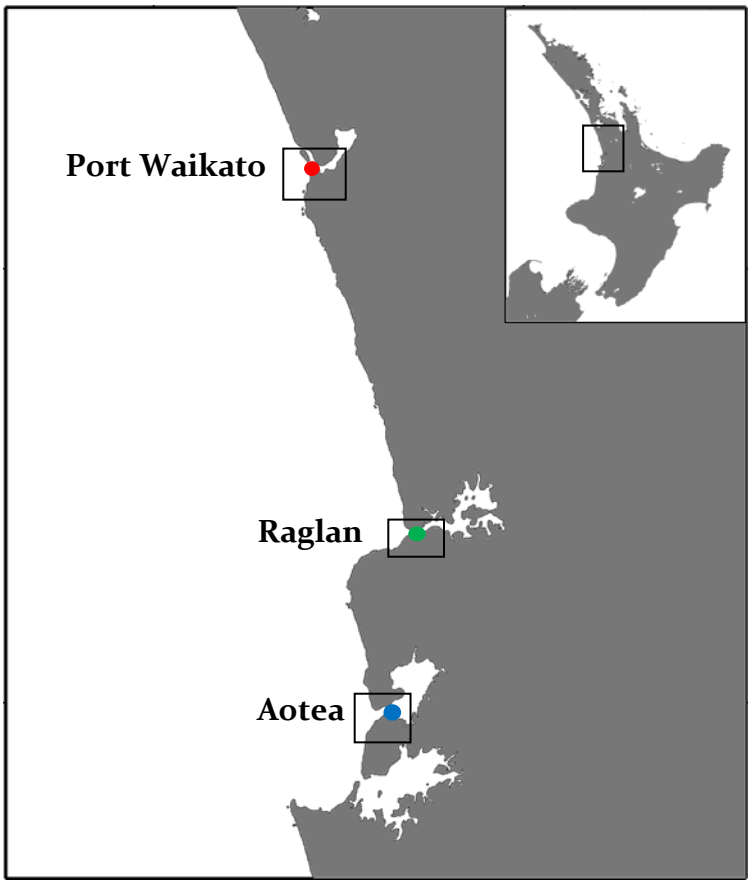

Figure 1.1 The location of Port Waikato (red dot), Raglan (green dot) and Aotea (blue dot) on the west coast of the Waikato Region, North Island, New Zealand. Boxes bounding the coloured dots indicate the extents of the three model C grids.

1.2 Review of Recent and Historic Literature

As noted above, this study extends the work of Power *et al.* (2011) and Goff and Chagué-Goff (2015) and provides tsunami wave height estimates for additional areas along the Waikato west coast for both regional and far-field sources.

Important results that came from the Power *et al.* (2011) study include:

- The Tonga-Kermadec Trench has produced two subduction thrust events of ~M8.0 in the last century and GPS data suggests that strong interseismic coupling to approximately 30 km depth may be indicative of the potential for larger (>M8.0) events to occur there.

- Based on thrust events on the Kermadec Arc between 1976 and 2009, the frequency of occurrence of earthquakes greater than or equal to M8.0 is about once per century on average.

- Numerical results for a M8.9 tsunami generated on the middle portion of the Kermadec subduction margin indicate that wave amplitudes of 3 – 5 m occur on the south-western coast of Northland. A result of the merging of separately

diffracted wave chains around the top of the North Island. In particular, fast-moving diffracted waves travelling through the South Norfolk and Reinga Basins catch up to the slow-moving diffracted waves travelling between Great Island (Three Kings Islands) and Cape Reinga.

- The Southern New Hebrides Trench produced a large ~M8.4 earthquake in 1901 and is shown to converge at a rate of 48 – 50 mm/year.

- Based on thrust events on the Southern New Hebrides Arc between 1976 and 2009, the frequency of occurrence of earthquakes greater than or equal to M8.0 is about once every 28 years on average.

- Numerical results for a M8.8 tsunami generated on the Southern New Hebrides subduction margin indicate that wave amplitudes of 3 – 5 m occur on the south-western coast of Northland. This effect is larger than that on Northlands east coast because of the wave-guiding effects of the Norfolk and Three Kings Ridges (see Figure 1.2).

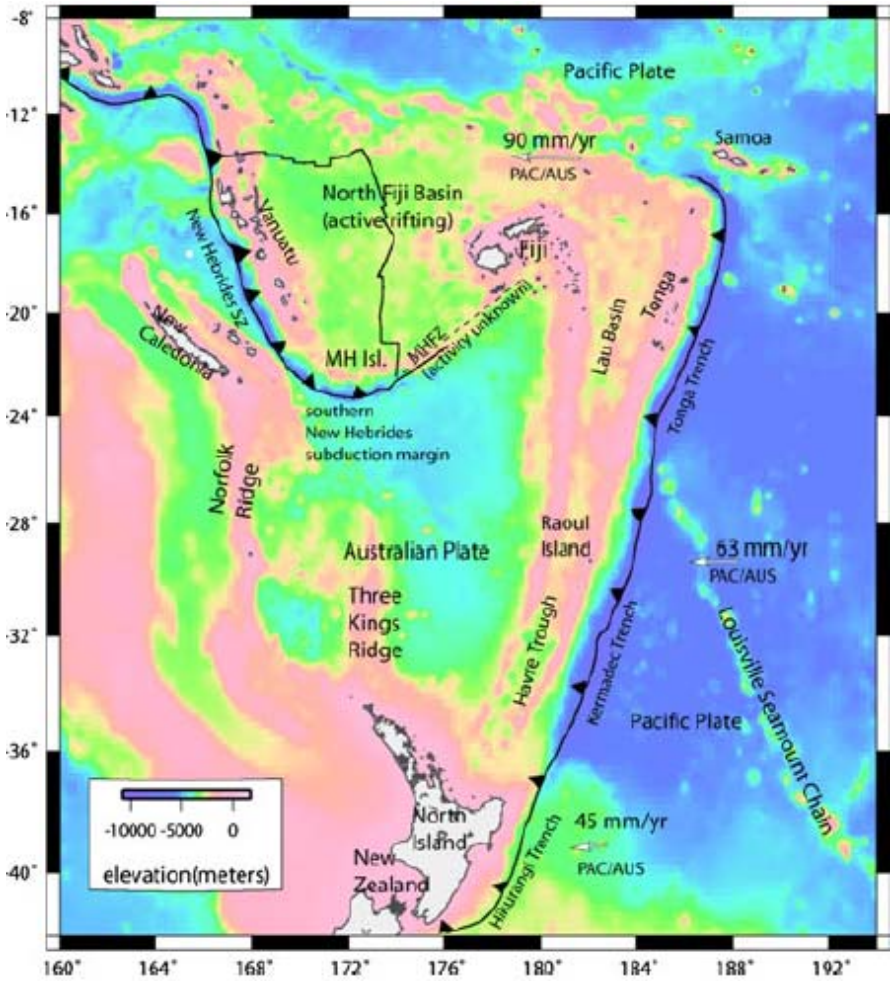

Figure 1.2 Tectonic setting of the Kermadec and New Hebrides plate margins. Black triangles signify the over-riding plate at the regions' subduction margins. White arrows show predicted motion of the Pacific Plate relative to the Australian Plate (taken from Power et al. (2011)).

Important results from the Goff and Chagué-Goff (2015) study include the identification of three (possibly 4) separate tsunami events along the west coast of New Zealand. These include an event in the modern era (August 1870) in Westport that was possibly misidentified and mis-associated with a tsunami that occurred in August 1868 and was caused by the great 1868 Arica Earthquake in Northern Chile and Southern Peru. A newspaper account of the event written in 1912 describes a significant series of waves starting as a 'huge bank of water about 40 feet high' that rushed up the river, retreating and returning two more times resulting in the destruction of several buildings and businesses as well as the flooding of the local cemetery resulting in the uncovering of and transport coffins. This event was believed to have occurred in 1868 as a result of the 1912 account stating that the year of the event's occurrence was "*when the Dominion of New Zealand was only twenty-seven years old*". As Goff and Chagué-Goff (2015) point out however, the 'Dominion of New Zealand' was only designated in 1907, however it became a separate British Crown colony in 1841, and this may be the reference year for the article thereby suggesting that the 'tidal wave' event occurred in 1868.

However, additional evidence presented by Goff and Chagué-Goff (2015) casts some doubt on the year in which this event occurred. This includes information from the register of New Zealand Historic Places Trust indicating that the building which housed the Bank of New South Wales in Westport was moved after it was "*inundated by a tidal wave in 1870*" before being relocated again in 1872 due to river flooding and ultimately destroyed a few years later by another river flood before being rebuilt in 1877 at a safer site. This evidence is important since it clearly differentiates between river flooding and the 'tidal wave' that first damaged the building. Also, it notes 1870 as the year for the 'tidal wave event' event, thus suggesting that the 1912 newspaper account was written by someone who confused the 1868 tsunami (which was well observed throughout New Zealand) with this unique one-off event in 1870. Interestingly, the Sydney tide gauge does show that a tsunami of negligible height and of unknown origin was recorded on August 12, 1870 (Goff and Chagué-Goff, 2014).

These details not withstanding, based on our modern understanding of tsunami wave propagation and far field effect, it is highly unlikely that the 1868 Arica earthquake and tsunami was capable of producing ~12 m, highly destructive surges in Westport. On the other hand it does seem strange that such a destructive and unusual event (destruction of several buildings, businesses, wharves and the cemetery!) did not garner more accurate, descriptive or widespread contemporary accounts. There fore, the source mechanism for this event remains a mystery. Given the extreme, highly localised wave heights, the very small tsunami height recorded in Sydney and the fact that there were no earthquakes recorded nearby on that day, points to a submarine landslide as a possible mechanism. Goff and Chagué-Goff (2015) point to slope failures on the Gilbert Seamount or within the Cook Canyon as possible sources, however no detailed studies on these sources have been conducted.

The fact that a relatively large and destructive, yet highly localized tsunami occurred on the west coast of New Zealand is in itself troubling. However, Goff and Chagué-Goff (2015) go on to describe evidence for two (or possibly 3) other events. One (or two) of these may have occurred in the South Taranaki Bight and and/or the

Westland Coast between 1470 and 1510 AD. The last event described by Goff and Chagué-Goff (2015) and most relevant to this study is that which may have occurred on the west Waikato coast between 1320 and 1450 AD affecting approximately 150 km of coastline between Albatross Point and Waikawau. A marked central region exists around Marokopa where most estimated wave run-ups are ~30 m above sea level and decrease significantly over 30 – 50 km alongshore to the north and south. This event is troubling in that it corresponds to extreme tsunami runup heights (~60 m maximum at Ngararahae) and because identifying a likely source for the wave is very difficult.

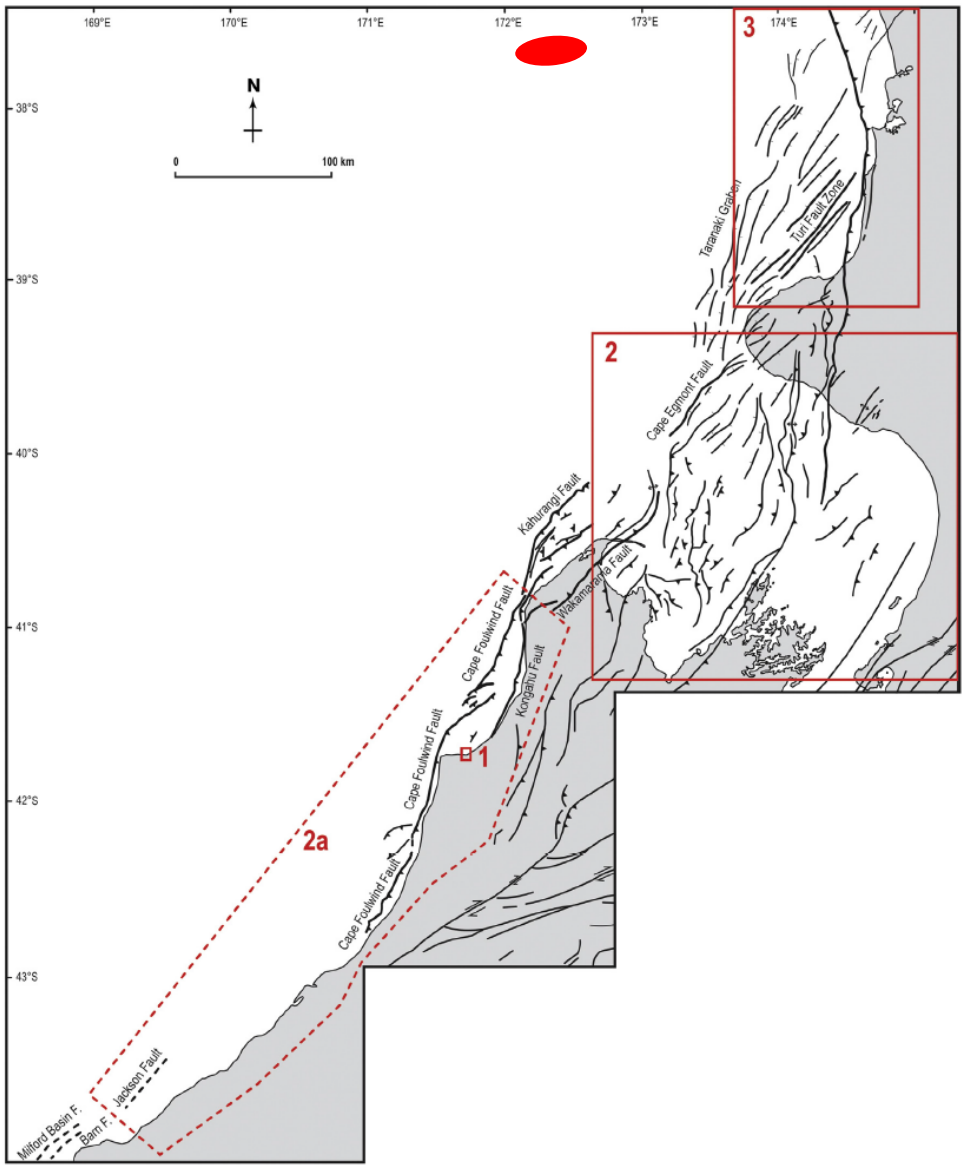

Figure 1.3 Main faults of the central west coast of New Zealand (taken from Goff and Chagué-Goff (2015)). The red ellipse indicates the approximate location of the Aotea seamount (37.6˚ S, 172˚ E)

While the distribution of the estimated runup heights corresponds to that created by a submarine slope failure, the local bathymetry does not contain significant slope failure source regions. Goff and Chagué-Goff (2015) point to the Aotea Seamount as a possible source, however they note that this feature rises approximately 1200 m

from the surrounding seafloor reaching its peak in approximately 1000 m of water. Given the scale of the Aotea Sea Mount and the depths in which it lies, it would require an extraordinarily large slope failure to generate an initial wave large enough to produce the 30 to 60 m on shore tsunami heights. We assess this with a numerical modelling study in Section 5 below.

As a final note, we point another tsunami event that may have occurred on the Waikato west coast and is described in de Lange and Healy (1986). They report that in June 1891: "*following an earthquake located offshore from the mouth of the Waikato River, the local Maori population reported that water within Aotea Harbour was greatly agitated and large waves were observed entering the harbour."*

However, there were no reports from Raglan or Manukau Harbours and official reports from Manukau Harbour "*make no mention of unusual tides".*

1.3 Modelling Approach

The numerical modelling presented in this study was carried out using the Community Model Interface for Tsunamis (ComMIT) numerical modelling tool. The ComMIT model interface was developed by the United States government National Oceanic and Atmospheric Administration's (NOAA) Centre for Tsunami Research (NCTR) following the December 26, 2004 Indian Ocean tsunami as a way to efficiently distribute assessment capabilities amongst tsunami prone countries.

The backbone of the ComMIT system is a database of pre-computed deep water propagation results for tsunamis generated by unit displacements on fault plane segments (100 x 50 km) positioned along the world's subduction zones. Currently, there are 1,691 pre-computed unit source propagation model runs covering the world's oceans included in the propagation database. Using linear superposition, the deep ocean tsunami propagation results from more complex faulting scenarios can be created by scaling and/or combining the pre-computed propagation results from a number of unit sources (Titov *et al.,* 2011). The resulting trans-oceanic tsunami propagation results are then used as boundary inputs for a series of nested near shore grids covering a coastline of interest. The nested model propagates the tsunami to shore computing wave height, velocity and overland inundation. The hydrodynamic calculations contained within ComMIT are based on the MOST (Method Of Splitting Tsunami) algorithm described in Titov and Synolakis (1995, 1997) and Titov and Gonzalez (1997). The ComMIT tool can also be used in conjunction with real time recordings of tsunami waveforms on one or more of the deep ocean tsunameter (DART) stations deployed throughout the oceans to fine tune details of an earthquake source mechanism in real time. An iterative algorithm that selects and scales the unit source segments is used until an acceptable fit to the observed DART data is met.

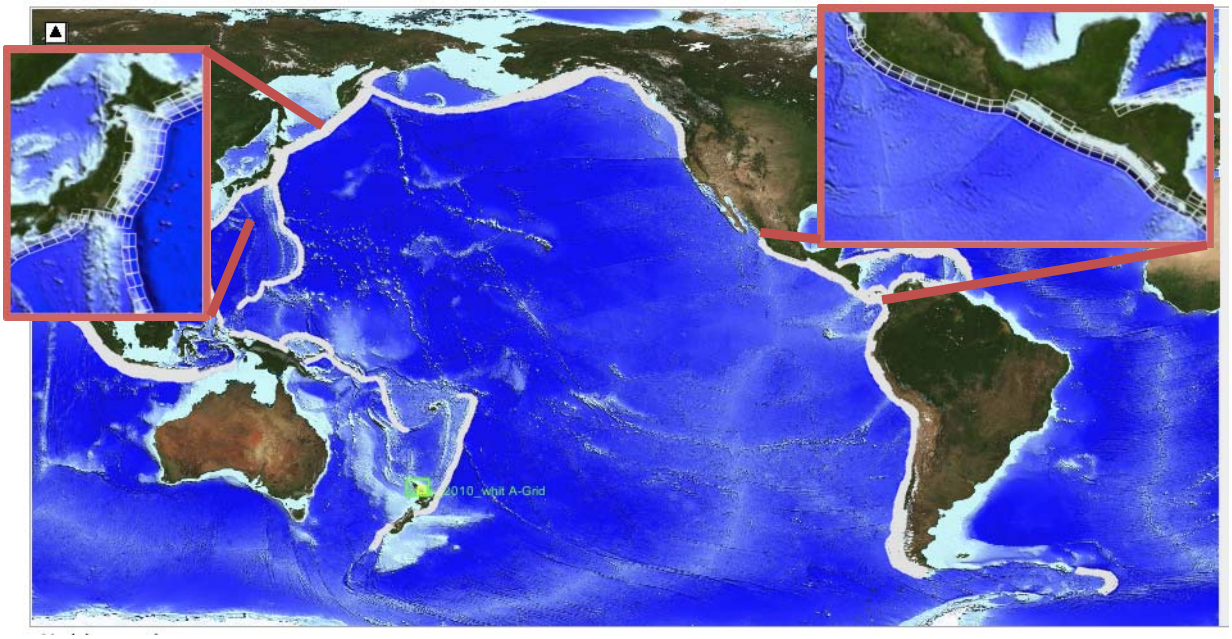

Figure 1.4 The ComMIT propagation model database for tsunamis in the world's oceans. Insets show the details of the source zone discretization in to rectangular sub-faults.

1.4 Numerical Modelling Grids

The Waikato Regional Council (WRC) provided raw bathymetry and LiDAR topography data for construction of the numerical modelling grids. The data were provided with a reference datum of MSL, a WGS84 projection and were combined with additional data sets covering the regional offshore bathymetry and on land topography. This included the Shuttle Radar Topography Mission (SRTM) 90 m resolution topography and nautical chart data from Land Information New Zealand (LINZ). An additional survey dataset of the Port Waikato central channel, also supplied by WRC, was used to complement the LiDAR there. The coverage areas of the various datasets are shown in Figure 1.5. The data were combined in to a master set of “x, y, z” triplets and then gridded in to different resolutions and coverage areas using a Kriging algorithm. The highest resolution C level model grids (10 m) are shown in Figure 1.6. Model grids were set up for both mean sea level (MSL) and mean high tide (HT).

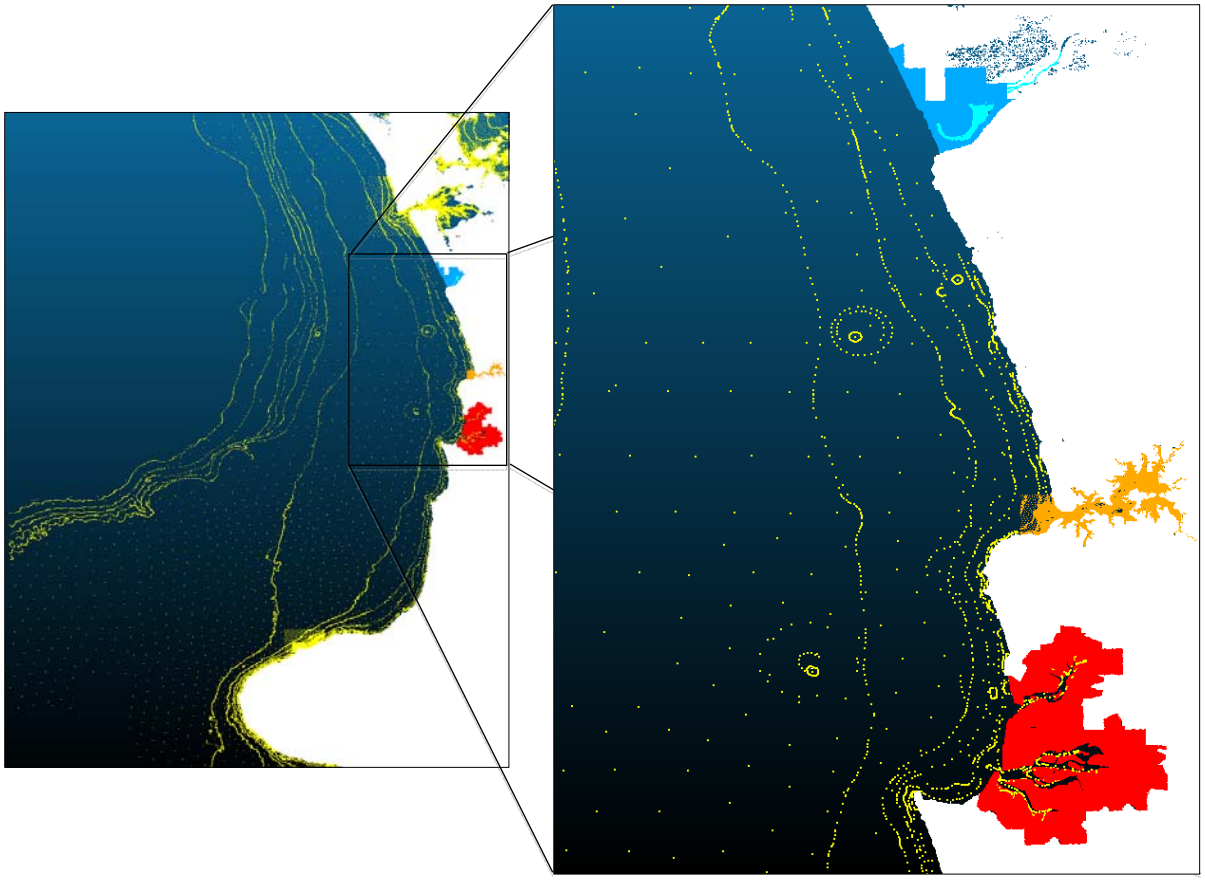

Figure 1.5 Coverage area of the different bathymetry data sets. White: SRTM topography, Yellow: LINZ digitised chart contours and sounding points, Red, Orange and Blue: LiDAR topography, Light Blue: WRC survey.

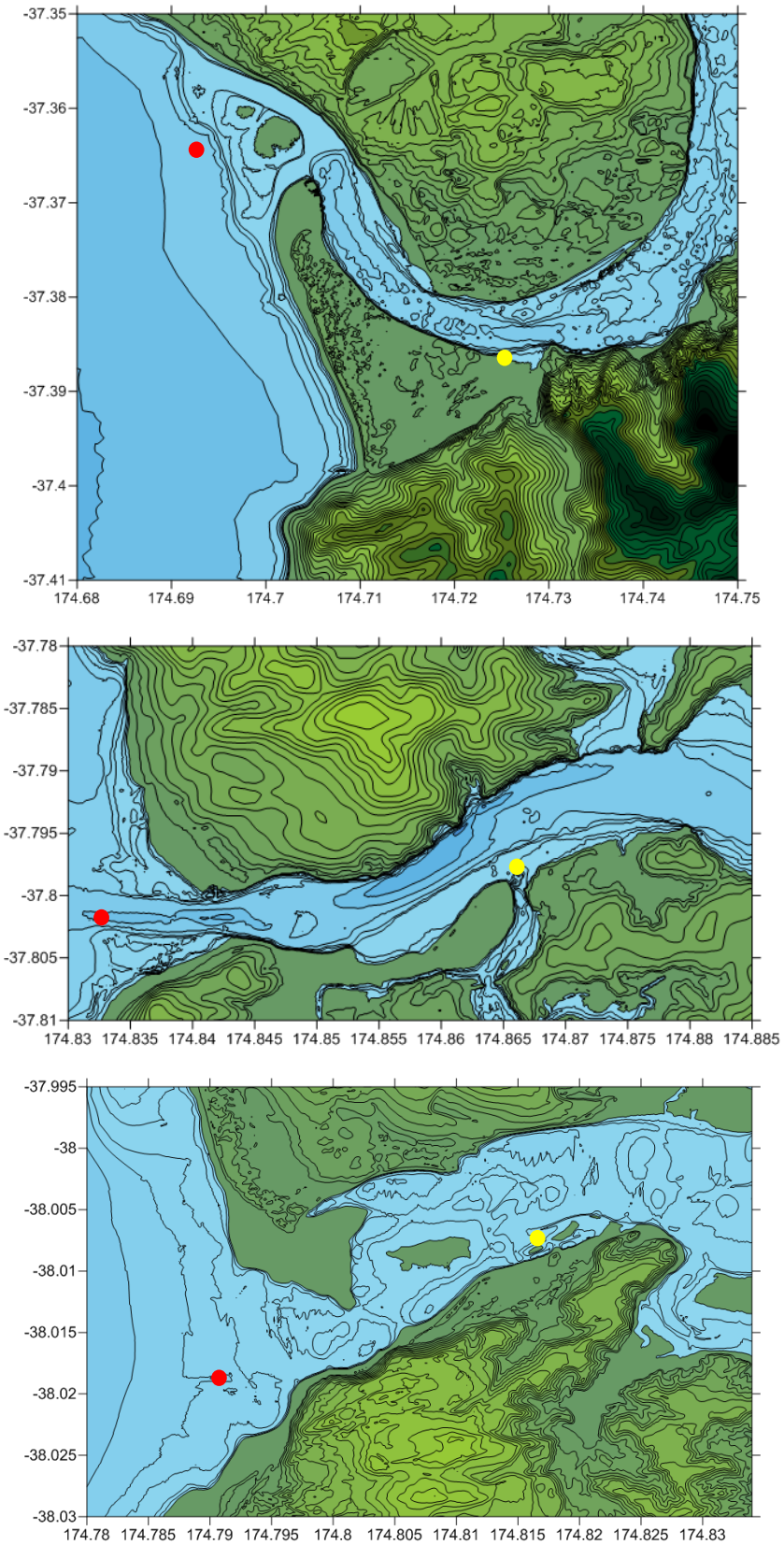

Figure 1.6 The final numerical modelling C grids (MSL) at 10 m resolution: Port Waikato (top), Raglan (middle) and Aotea (bottom). The red and yellow dots indicate the locations where water level time-series are extracted outside and inside each harbour respectively.

1.5 Aotea Harbour Bathymetry

It should be noted that the LiDAR data used to build the Aotea Harbour modelling grid was based on data collected in 2007-2008. As a result, the bathymetry does not reflect the current configuration of the northern spit at the entrance to Aotea Harbour. Changes in the morphology of the Aotea Harbour entrance are presented in Figure 1.7 and Figure 1.8. It is apparent that the data used here satisfactorily represents the shape of the northern spit in 2008, however significant changes are apparent over subsequent years. As of the most recent image (August 2015) the spit appears to be returning to the general shape seen in the 2008 imagery and data.

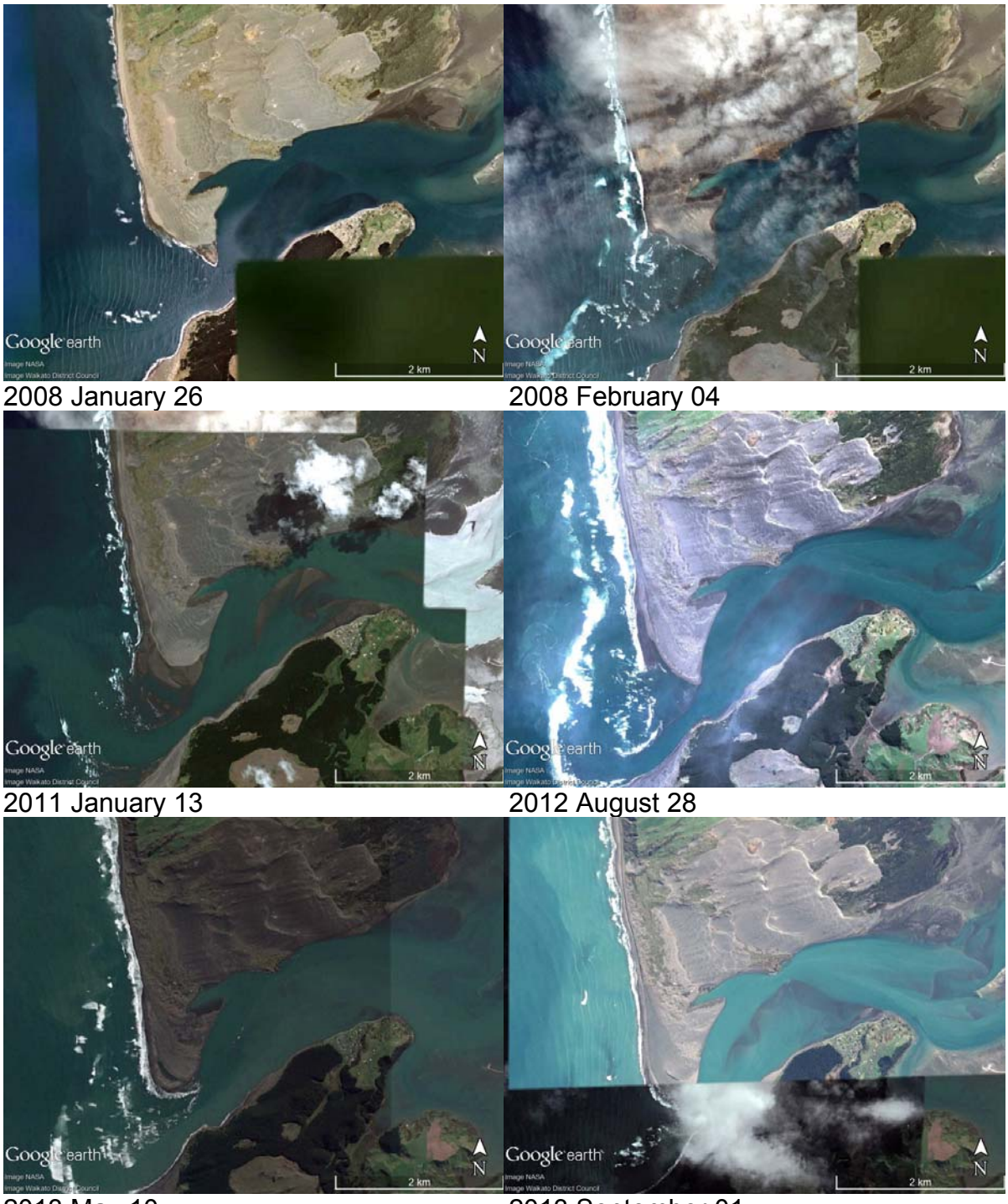

Figure 1.7 Changes in the morphology of the Aotea Harbour bar from 2008 - 2013

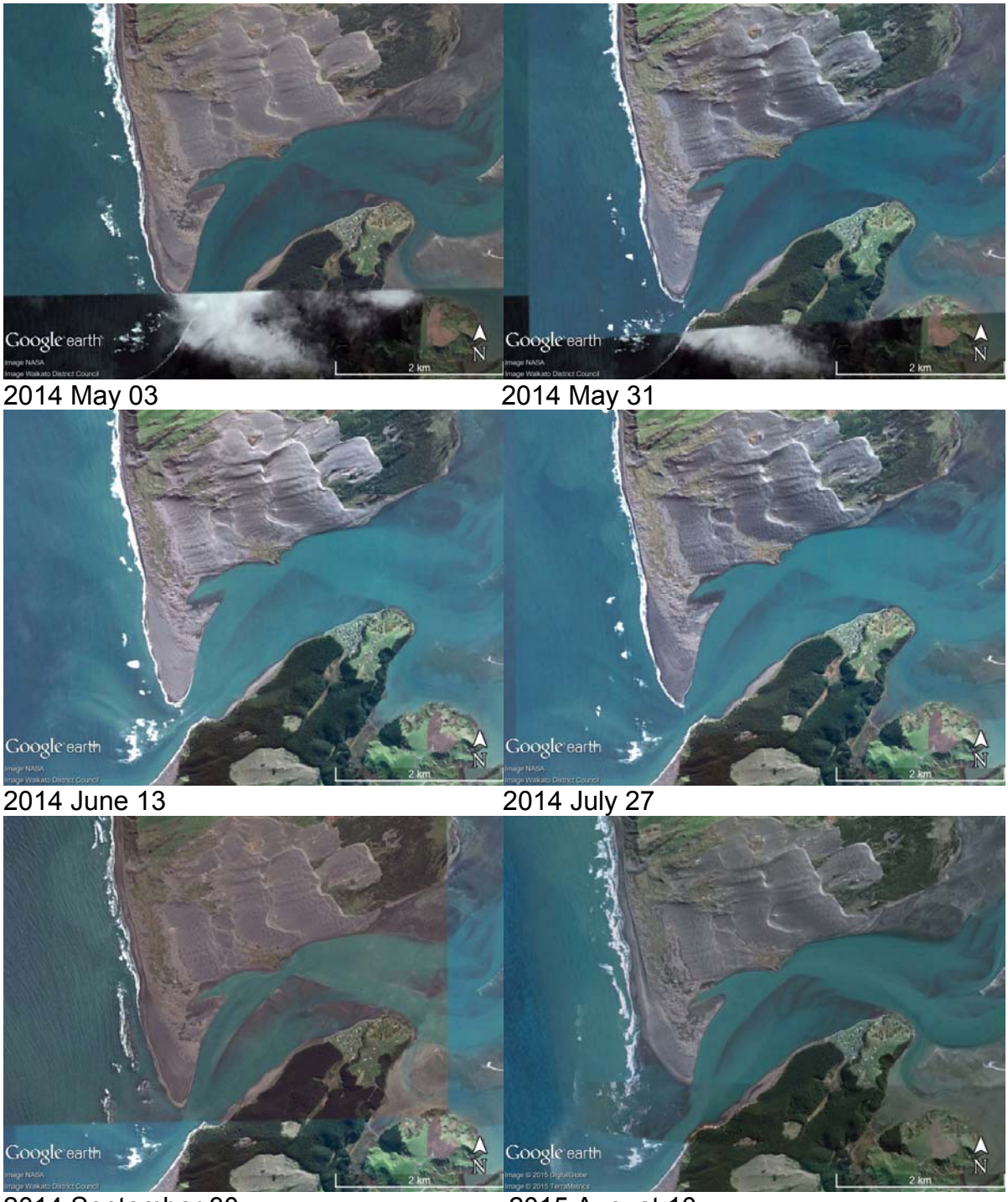

2014 May 03 2014 May 31

2014 June 13 2014 July 27

2014 September 30 2015 August 10

Figure 1.8 Changes in the morphology of the Aotea Harbour bar from 2013 - 2014

2 TSUNAMI SOURCE MODELS

For this study we focus on tsunamis generated by tectonic sources on both regional and far-field subduction zone plate margins. For the regional sources we use a suite of hypothetical earthquake scenarios of with magnitude M 9.0 positioned on the southern New Hebrides, Tonga-Kermadec and Puysegur Trenches, (Figure 2.1).

A similar approach is used for tsunami sources in the Solomon Islands, while these tsunamis strictly speaking are 'distant source' due to the >5 hr travel times to our study sites, for geographic consistency, we group them with the regional sources below.

We also explore the effects of distant sources tsunami including the 1960 Valdivia, Chile earthquake and the 1868 Arica Chile earthquake.

2.1 Regional/Distant Source Scenarios in the South-western Pacific

These tsunami sources are based on the assumption that any subduction zone on earth is capable of producing a very large (i.e. M_W 9.0) earthquake. Although the subduction zones investigated in this study have not produced such large events in historical times, the possibility of such an event occurring cannot be discounted. Indeed the recent very large earthquakes occurring on the Sumatra subduction zone in December 2004 and offshore of northern Japan in March 2011 were not considered as plausible events based on historical seismicity and our present seismological understanding of these source regions.

As noted above, Power et al. (2011) studied the tsunami hazard for New Zealand from the Tonga-Kermadec trench and the southern New Hebrides subduction zone. In their assessment they also used hypothetically large earthquakes as the tsunami source with a M 8.8 event on the southern New Hebrides Trench and up to a M 9.4 event on the Tonga-Kermadec Trench. Here we adopt a similar approach, however we use a suite of identical earthquake sources positioned along the different subduction zones as indicated in Figure 2.1. Each tsunami source is represented by an earthquake with a fault plane area of 400x100 km and 22 m of uniform slip, corresponding to an earthquake with magnitude of M9.

Table 2.1 Regional tsunami sources used for the study.

Case Number	Name	Code
1	Southern New Hebrides	HEB 1
2	Puysegur Trench	PUY 1
3	Tonga-Kermadec south	TK 1
4	Tonga-Kermadec north	TK 2
5	Solomon Islands East	SOL 1
6	Solomon Islands Central	SOL 2
7	Solomon Islands West	SOL 3

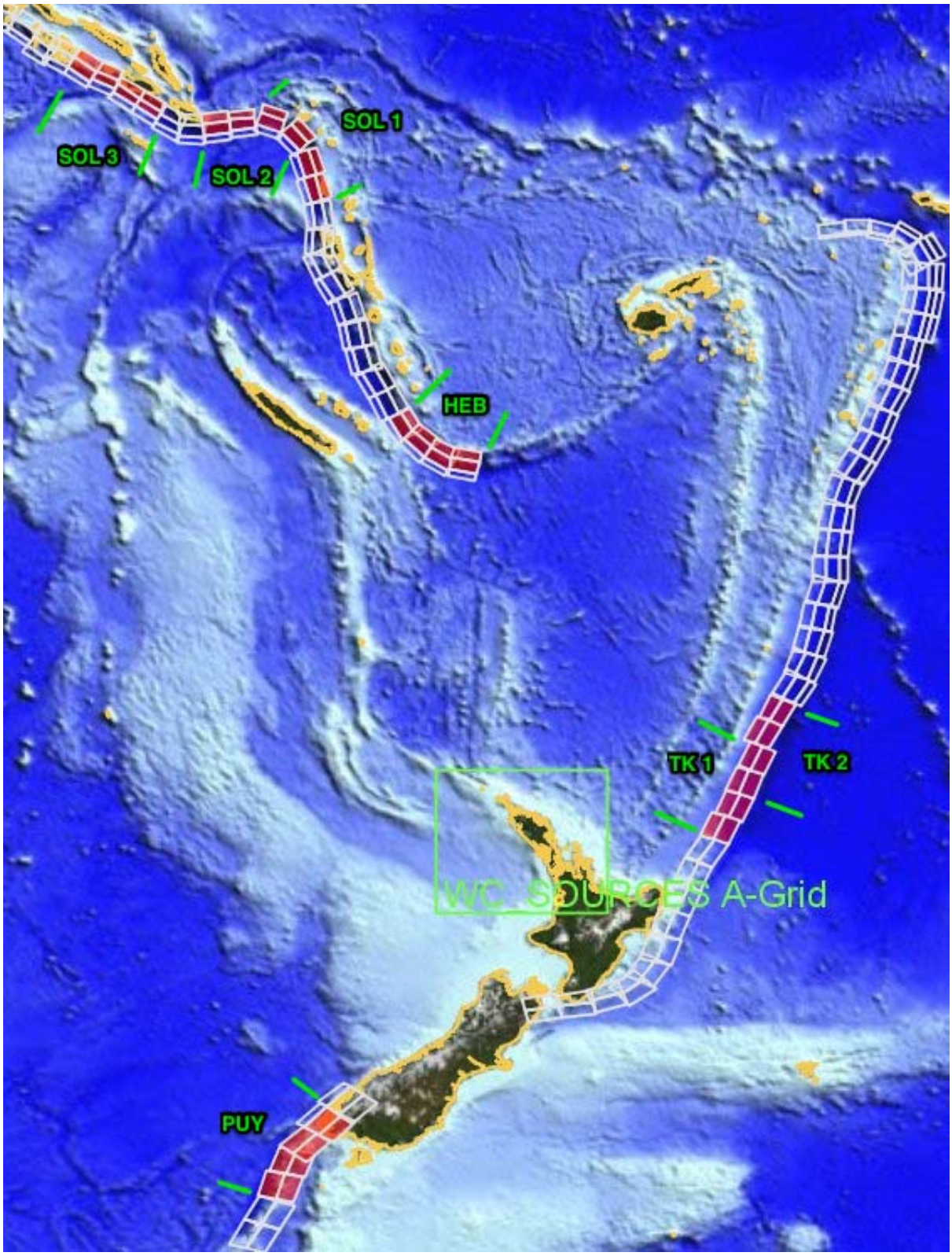

Figure 2.1 Regional tsunami source regions. *SOL* Solomon Trench, *HEB* New Hebrides Trench, *TK* Tonga-Kermadec Trench and *PUY* Puysegur Trench.

2.2 Distance Source Scenarios

In this report, two distant source tsunami scenarios are considered. These are based on the 1868 Arica and 1960 Valdivia historical Chilean events. The rationale for focussing on these two sources only is discussed in Section 4 below.

Borrero (2013) conducted a detailed analysis of the effects of the 1960 tsunami at Whitianga. In that study he compared the numerical model results from 6 different versions of the tsunami source for that event to eyewitness accounts and observations of inundation at Whitianga. The results of that study suggested that the earthquake slip distribution proposed by Fujii and Satake (2012) provided the best fit to the overall observed effects. However, it was necessary to increase the overall slip amounts by 20% to most accurately reproduce the observed inundation. The fault segments, initial seafloor deformation and slip amounts used for that source are shown in Figure 2.2 and Table 2.2.

For the 1868 Arica event, we used source segments corresponding to a rupture extending from Arica, Chile, 600 km northward into southern Peru. This source uses uniform slip of 39.6 m over the fault plane. This source mechanism produced the best fit to the available observations of the 1868 tsunami in Lyttelton Harbour as discussed in Borrero and Goring (2015).

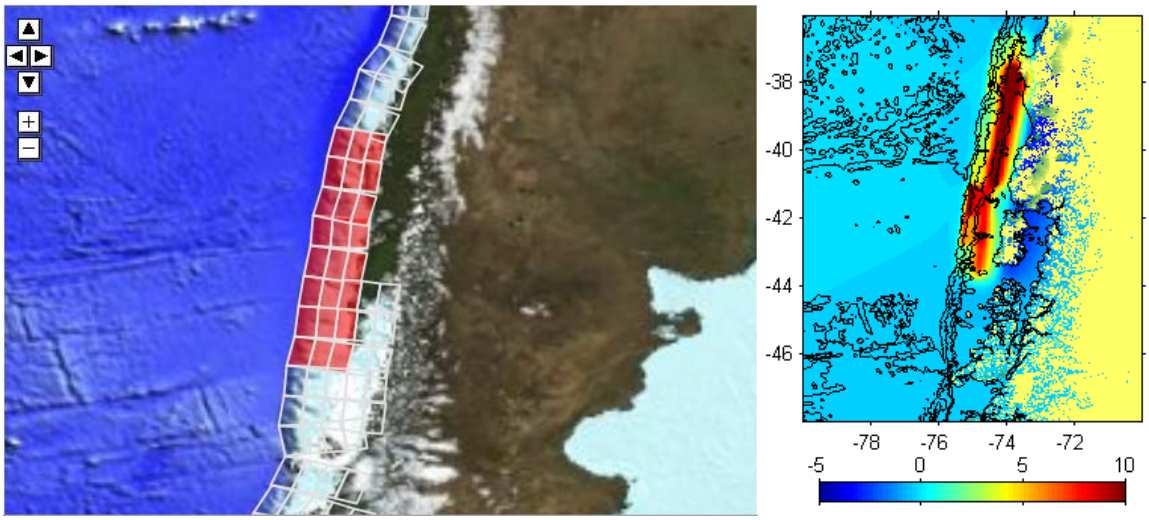

Figure 2.2 (left) Unit source segments used to define the 1960 Chilean Earthquake suite of events. (right) Initial sea floor deformation at the source region.

Table 2.2 Faults segment slip amounts for the 1960 Chilean tsunami.

Fault Segment Slip Amounts		
5.0	12.9	1.2
6.6	36.1	21.0
2.8	31.1	11.3
4.9	29.6	11.5
7.8	32.9	6.6
25.7	17.8	6.2
15.3	21.7	5.5
3.7	20.5	2.7

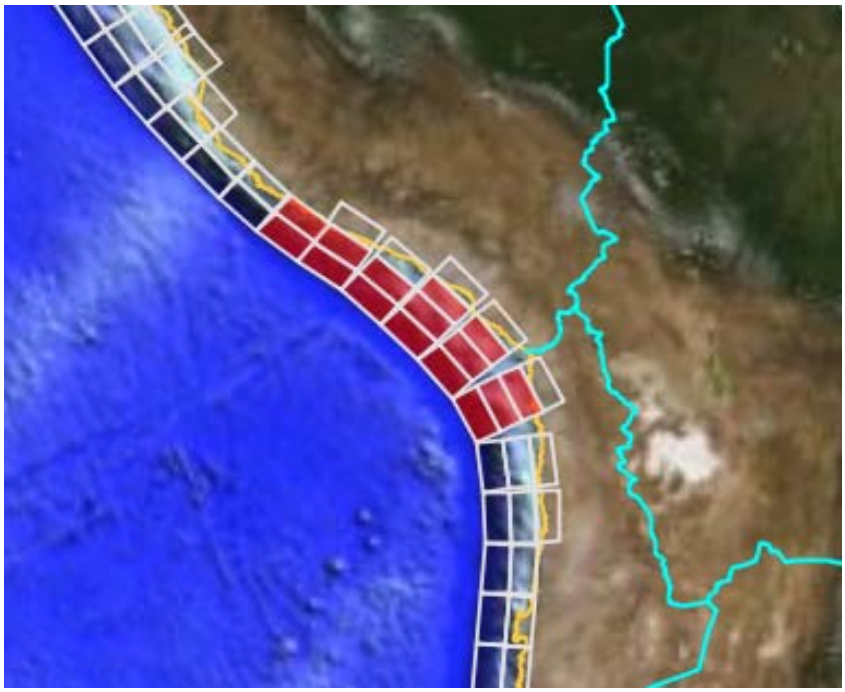

Figure 2.3 Source segments used for the 1868 Arica tsunami.

3 MODEL RESULTS: REGIONAL/DISTANT TSUNAMIS SOURCES IN THE SOUTHWESTERN PACIFIC

3.1 Propagation Models

Tsunami water levels and current speeds for the sources described above were modelled at Port Waikato, Raglan and Aotea. For each of the cases, we have plotted the modelled tsunami wave heights in the southwest Pacific (Figure 3.1 and Figure 3.2). The regional propagation plots show the strong influence bathy metric features have on guiding tsunami wave energy towards the west coast. This is particularly true for the three Solomon Islands cases with the Solomon 3 cases showing a strong focussing effect along the Lord Howe Rise (Figure 3.2). Also evident is how the west coast is largely shielded from the brunt of the wave energy produced by either of the two Tonga-Kermadec trench sources. From these plots we can also see that the Puysegur source transmits significant tsunami wave energy toward the west coast despite its southerly position and near parallel orientation relative to the west Waikato coastline.

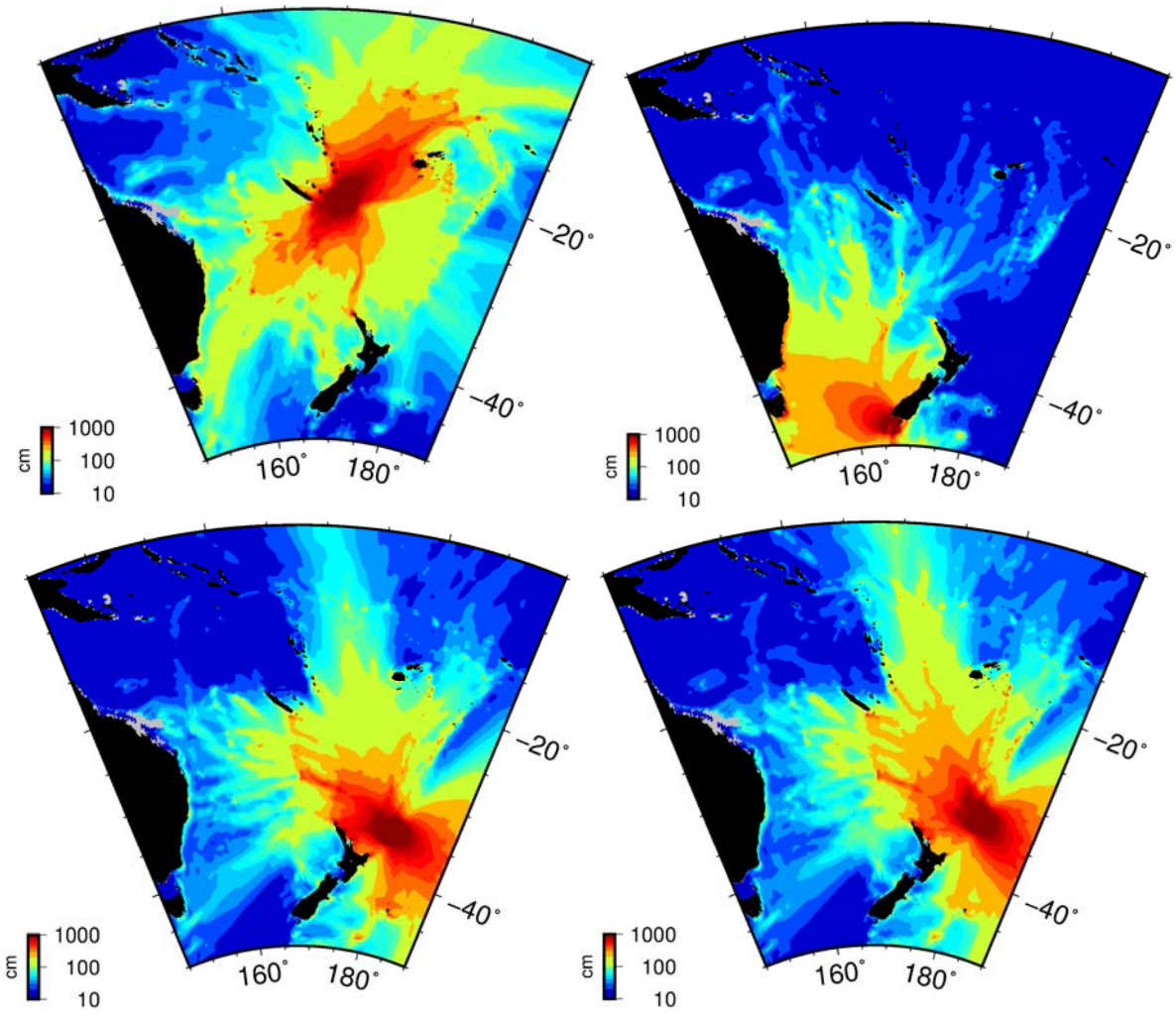

Figure 3.1 Maximum computed tsunami heights over the southwest Pacific region for the Southern New Hebrides (top left), Puysegur (top right), TK 1 (bot. left) and TK 2 (bot right) sources.

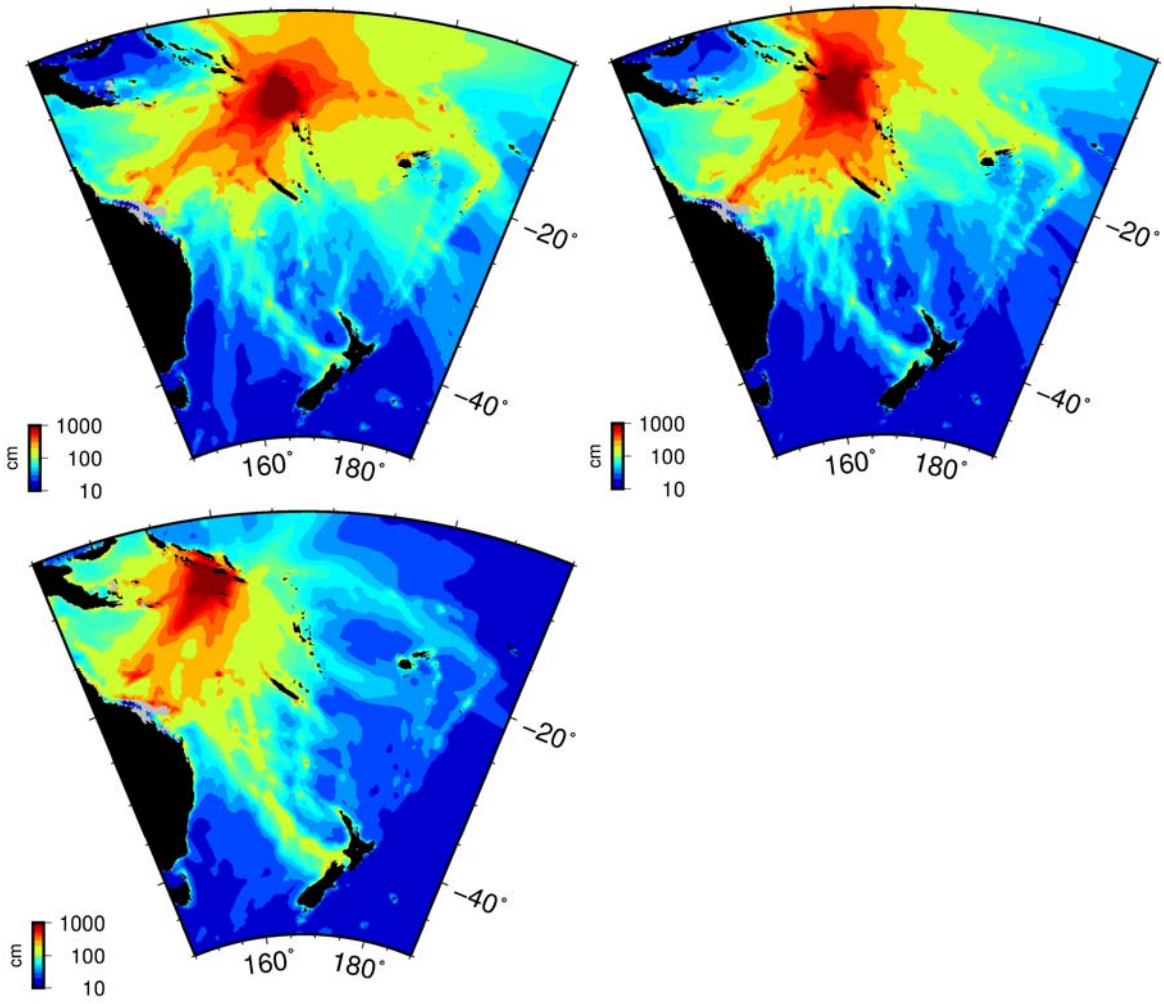

Figure 3.2 Maximum computed tsunami heights over the southwest Pacific region for the Solomon 1 (top left), Solomon 2 (top right) and Somolon 3 (bot. left) sources.

3.2 Tsunami Arrival Times and Heights

An important consideration for the regional tsunami hazard is a clear understanding of the tsunami arrival time. 'Tsunami arrival' however can be defined in a number of ways, whether it is the time of the first water level change (rise or drop) or the time of the maximum wave height.

As discussed above, tsunami sources are generally grouped according to the tsunami wave travel time from the source region to the site of interest. For the New Zealand context, Power (2013) groped sources according to the following definitions:

- Distant source – more than 3 hours travel time from New Zealand
- Regional source – 1–3 hours travel time from New Zealand
- Local source – 0–60 minutes travel time to the nearest New Zealand coast

For the different tsunami sources, we depict the tsunami arrival times and time series of the water levels throughout the tsunami simulations in Figure 3.4 through Figure 3.7. In these plots we see that the first withdrawal of the water surface begins approximately 3 – 3.5 hours after the earthquake for the Southern New Hebrides, Puysegur and two Tonga-Kermadec sources, and around 5 – 5.5 hours after the earthquake for the two Solomon sources.

Strictly speaking and using the definitions above, all of these events could be classified as 'distant source' relative to the west coast of the Waikato (just marginally so for the Tonga-Kermadec, Puysegur and Southern New Hebrides sources). However, since tsunamis from these source regions would be affecting other parts of New Zealand in much less time (i.e. Northland for the Solomon Islands and Southern New Hebrides, the Coromandel Peninsula and Bay of Plenty for the Tonga-Kermadec and Southland for the Puysegur Trench), and for geographic regions, we consider this group of sources to be 'regional' here.

For the first Tonga-Kermadec case at all three harbours, the initial withdrawal is followed by the largest positive surge (equal largest at Port Waikato), a result that is in line with that presented by Power *et al.* (2011) for the west coast of Northland. In contrast however, all other cases show that significant surges continue for several hours after tsunami arrival. Notably, the Solomon 1 scenario shows a significant surge occurring 14-15 hours after the earthquake. That this surge is not evident in the Solomon 2 scenario results is indicative of the strong role wave focussing and de-focussing over large bathymetric features has on tsunami induced water levels.

The timing of the tsunami first arrival, peak tsunami activity and largest tsunami surge are summarised in Table 3.1.

Plots of the maximum computed tsunami heights are presented in Figure 3.9 for the Solomon 1 and Puysegur tsunami sources. The complete set of modelled maximum tsunami heights are presented in the various appendices. The highest modelled tsunami heights across the simulations occurs for the Puysegur scenario. This scenario produces tsunami heights of up to 3.1 m at the shoreline just south of the entrance to Aotea Harbour, 3.0 m just north of the river mouth at Port Waikato and 2.4 m to the north of Raglan Harbour.

This Puysegur scenario is the only one that produces any appreciable overland inundation and in Figure 3.10 we present flow depth plots showing the extent and depth of the inundation for the three sites for this case. In general the inundation is limited to the beach areas of the open coast and does not affect the populated areas inside the harbours or up the river. The exception being the Kopua Domain area inside of Raglan Harbour where the model results suggest that this area is susceptible to flooding for the Puysegur scenario.

Table 3.1 Summary of Tsunami arrival and timing of peak tsunami activity for regional sources. All times are approximate and determined through visual inspection of the time series plots.

	First Arrival (hrs)	Peak Activity (hrs)	Largest Surge (hrs)
Port Waikato			
HEB	3.5	3.5-4	9
PUY	3	3-9	4.8
TK 1	3	3-12	6.5
TK 2	3	3-16	6.5
SOL 3	6	6-16	14
SOL 2	6	6-16	11
SOL 3	6	6-18	13
Raglan			
HEB	4	4-11	10
PUY	3.5	3.5-9	5
TK 1	3	3-12	3.5
TK 2	3	3-12	3.5
SOL 3	6	6-20	9
SOL 2	6	6-20	11
SOL 3	6	6-20	19
Aotea			
HEB	4	4-13	6
PUY	3.5	3.5-11	7
TK 1	3	3-14	3.5
TK 2	3	3-14	6
SOL 3	6	6-20	10
SOL 2	6	6-18	10
SOL 3	6	6-20	10

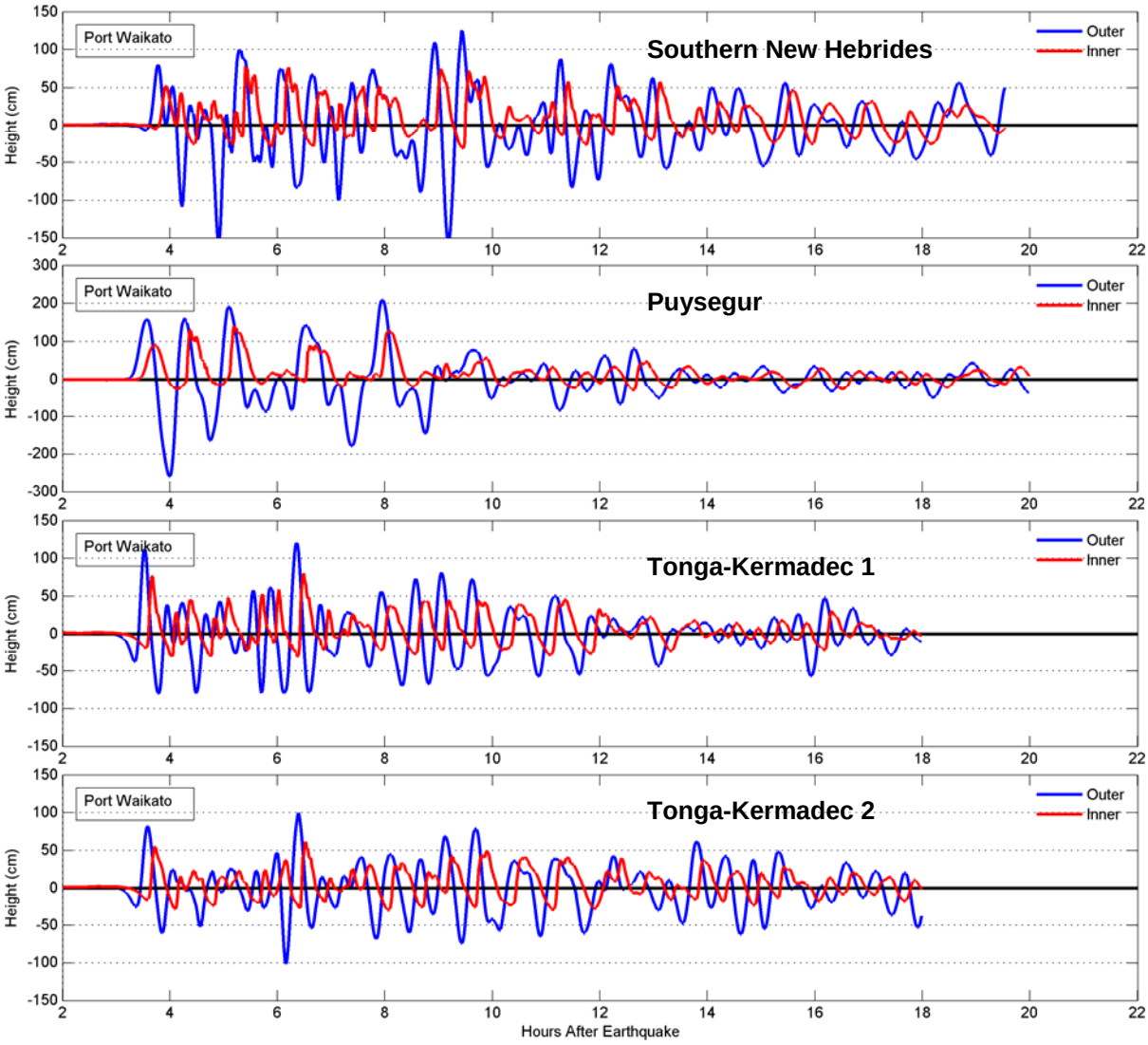

Figure 3.3 Water level time series plots for each regional source at Port Waikato. Top to bottom: New Hebrides, Puysegur, Tonga-Kermadec 1 and Tonga-Kermadec 2. Blue lines represent the outer harbour while red lines represent the inner harbour. Time series locations are indicated by the red and yellow dots in Figure 1.5. Note the different height axis for the Puysegur event.

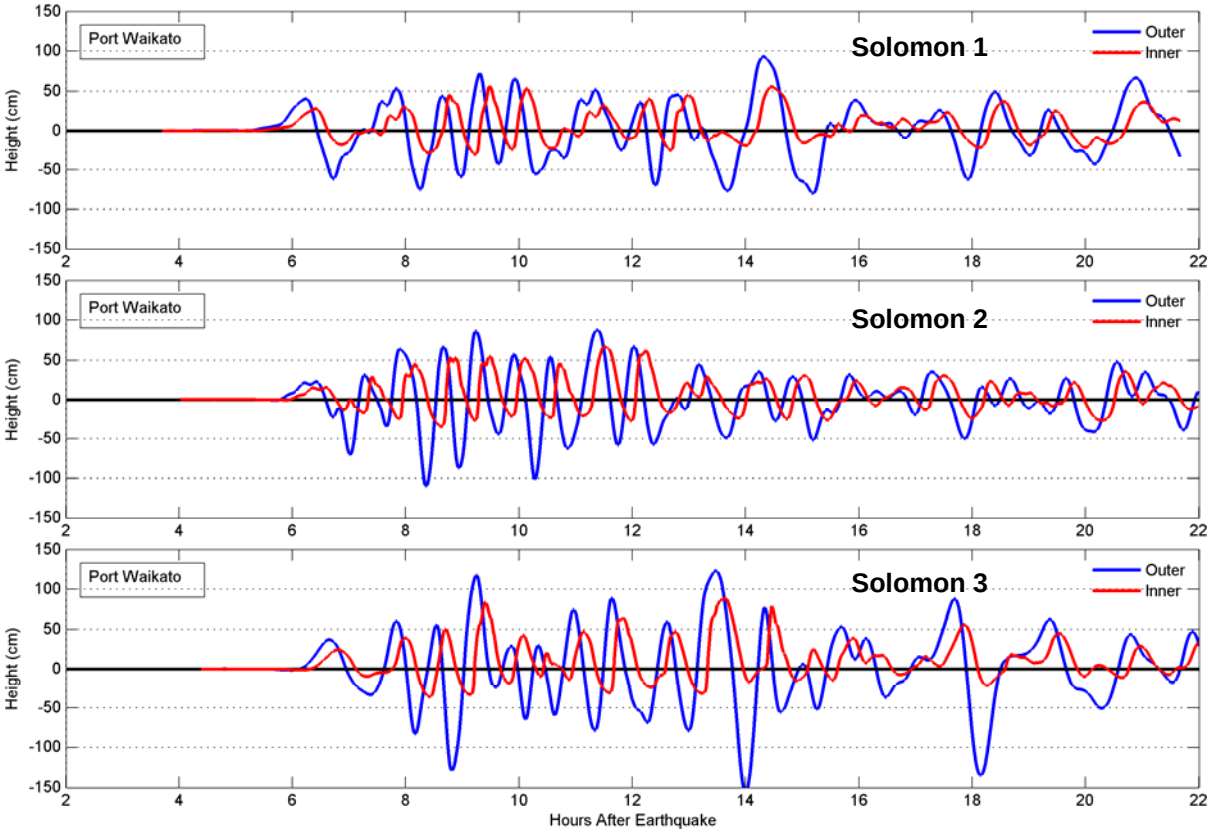

Figure 3.4 Water level time series plots for each regional source at Port Waikato. Top to bottom: Solomon 1, Solomon 2, Solomon 3. Blue lines represent the outer harbour while red lines represent the inner harbour. Time series locations are indicated by the red and yellow dots in Figure 1.5. Note the different height axis for the Puysegur event.

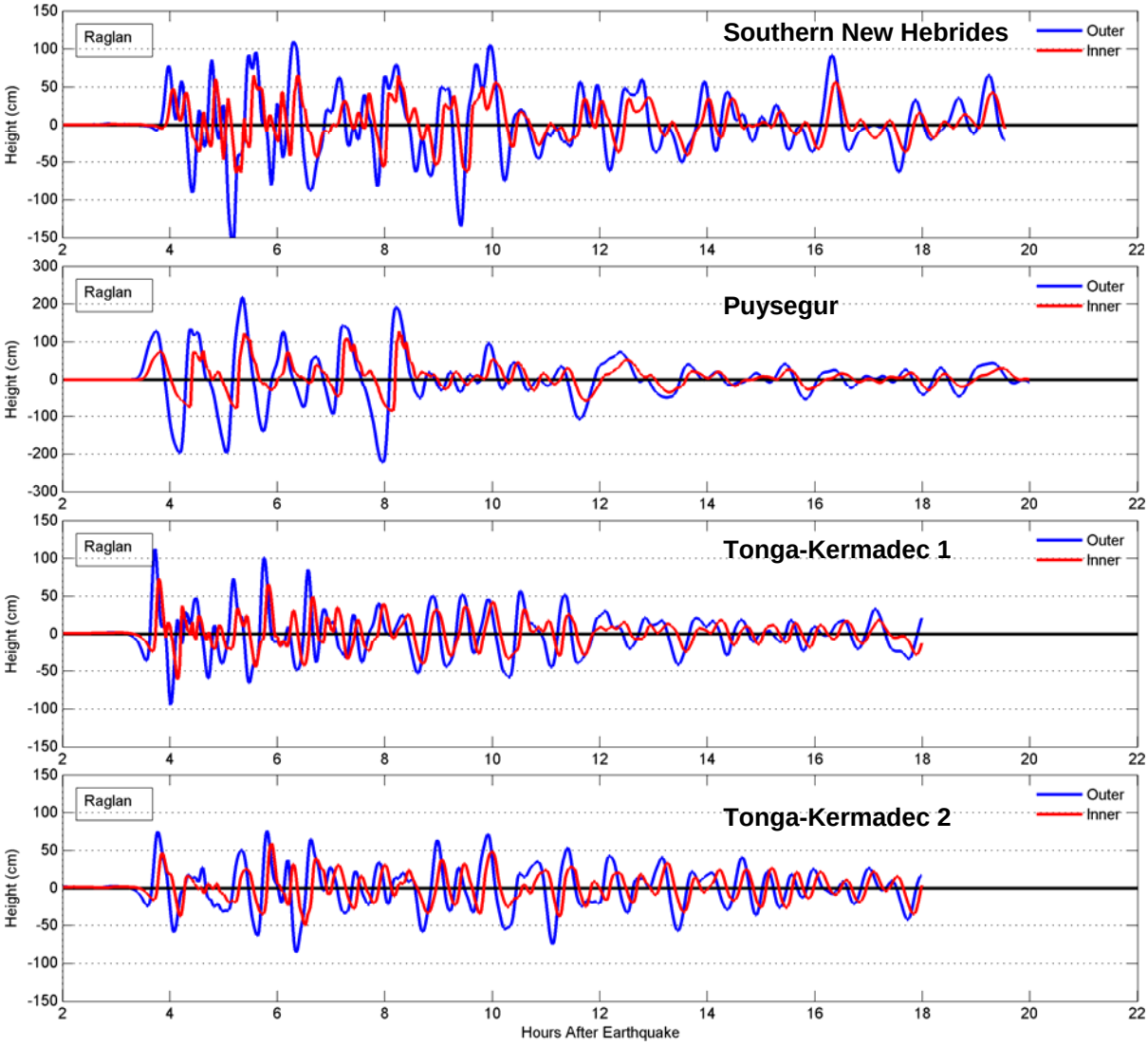

Figure 3.5 Water level time series plots for each regional source at Raglan Harbour. Top to bottom: New Hebrides, Puysegur, Tonga-Kermadec 1 and Tonga-Kermadec 2. Blue lines represent the outer harbour while red lines represent the inner harbour. Time series locations are indicated by the red and yellow dots in Figure 1.5. Note the different height axis for the Puysegur event

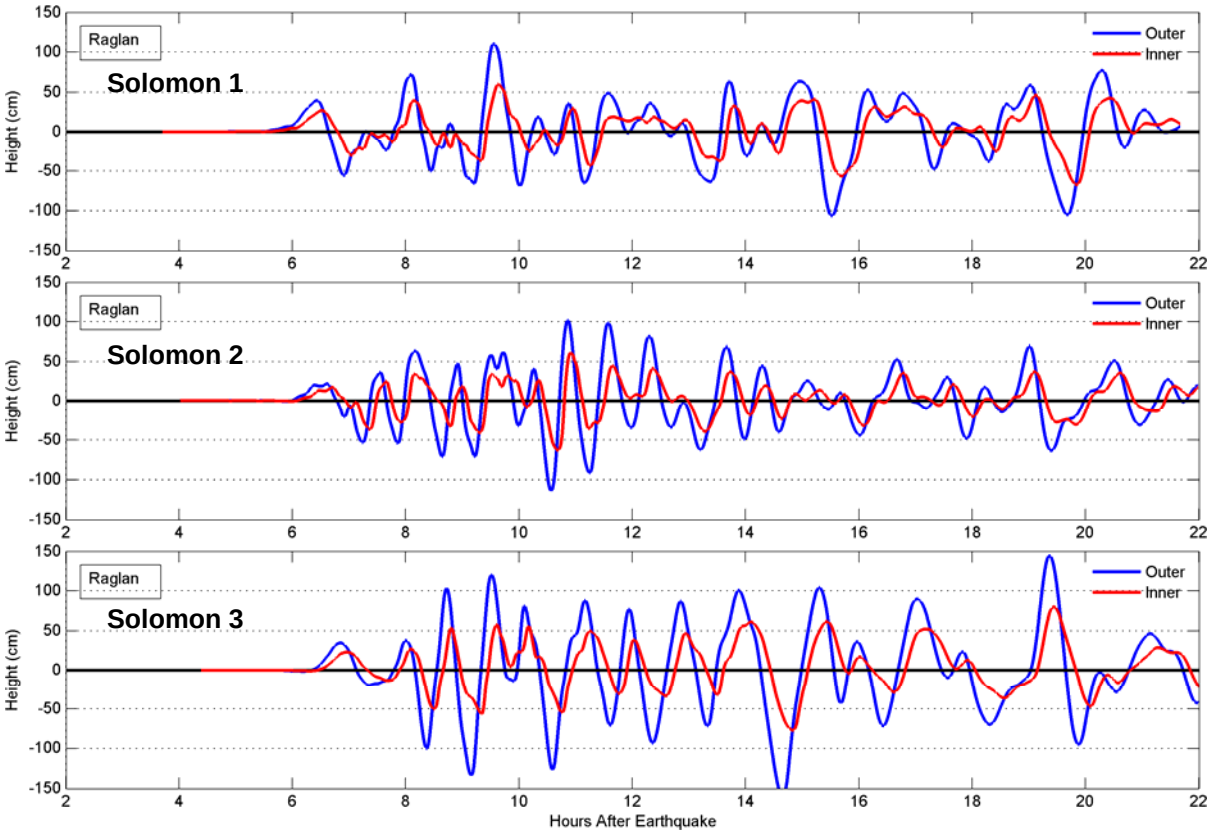

Figure 3.6 Water level time series plots for each regional source at Raglan Harbour. Top to bottom: Solomon 1, Solomon 2, Solomon 3. Blue lines represent the outer harbour while red lines represent the inner harbour. Time series locations are indicated by the red and yellow dots in Figure 1.5. Note the different height axis for the Puysegur event.

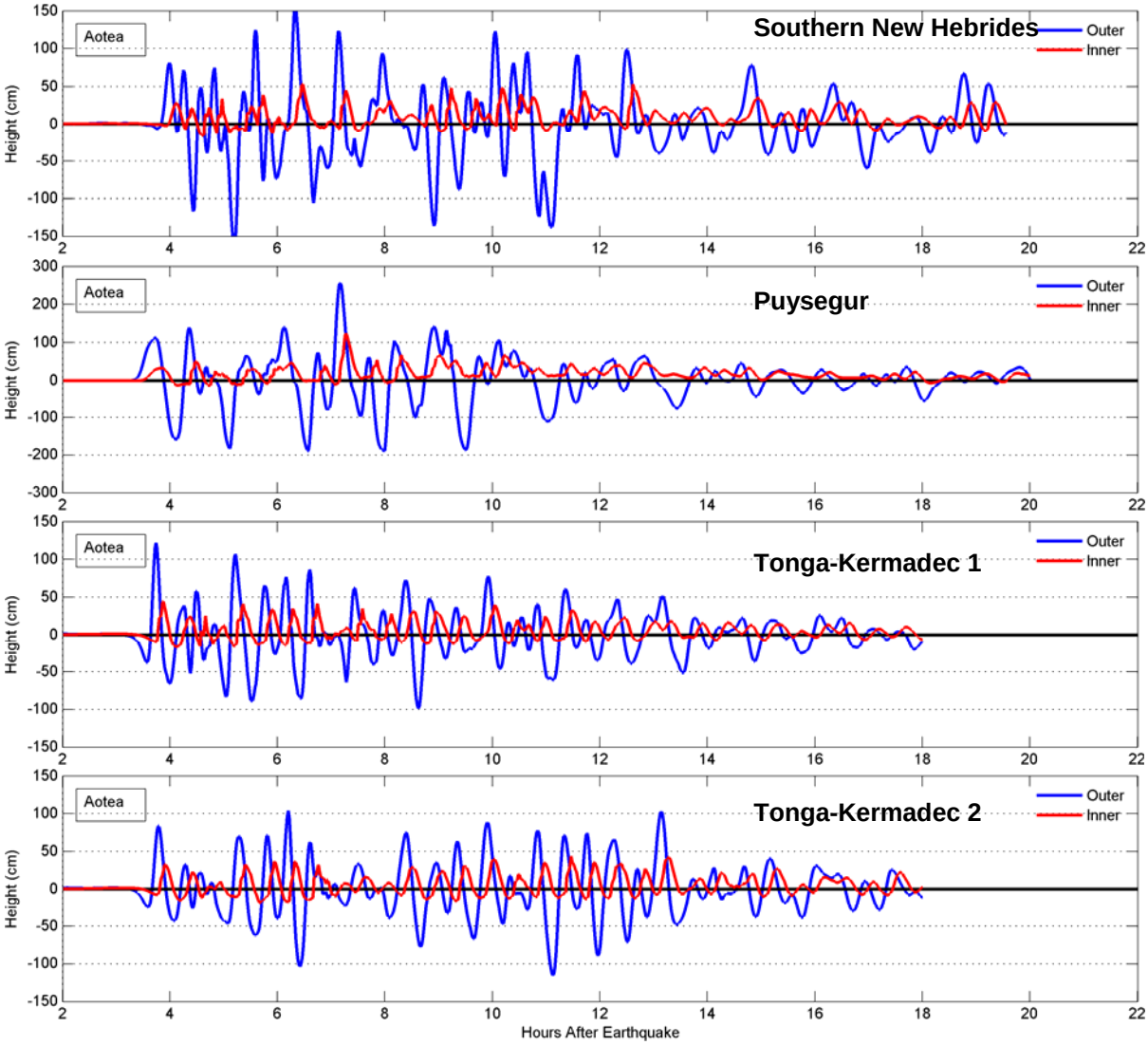

Figure 3.7 Water level time series plots for each regional source at Aotea Harbour. Top to bottom: New Hebrides, Puysegur, Tonga-Kermadec 1 and Tonga-Kermadec 2. Blue lines represent the outer harbour while red lines represent the inner harbour. Time series locations are indicated by the red and yellow dots in Figure 1.5. Note the different height axis for the Puysegur event

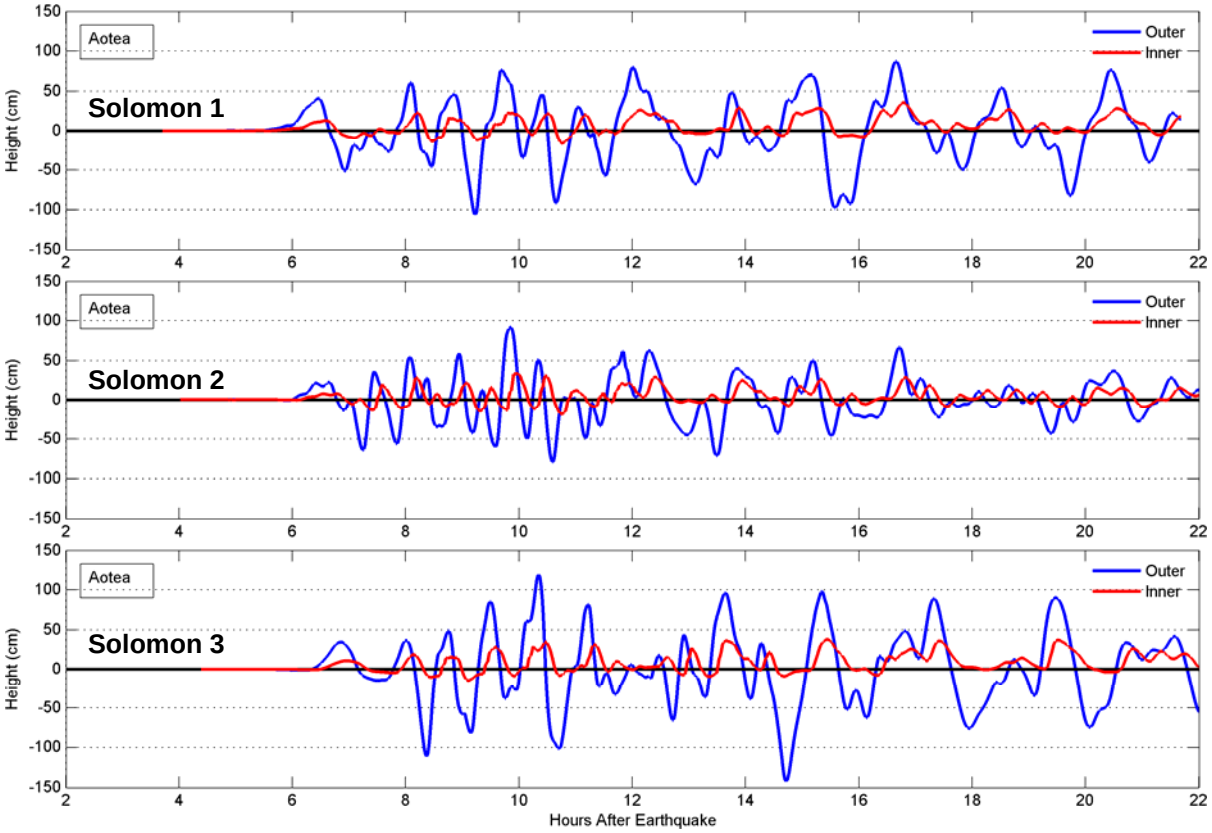

Figure 3.8 Water level time series plots for each regional source at Aotea Harbour. Top to bottom: Solomon 1, Solomon 2, Solomon 3. Blue lines represent the outer harbour while red lines represent the inner harbour. Time series locations are indicated by the red and yellow dots in Figure 1.5. Note the different height axis for the Puysegur event.

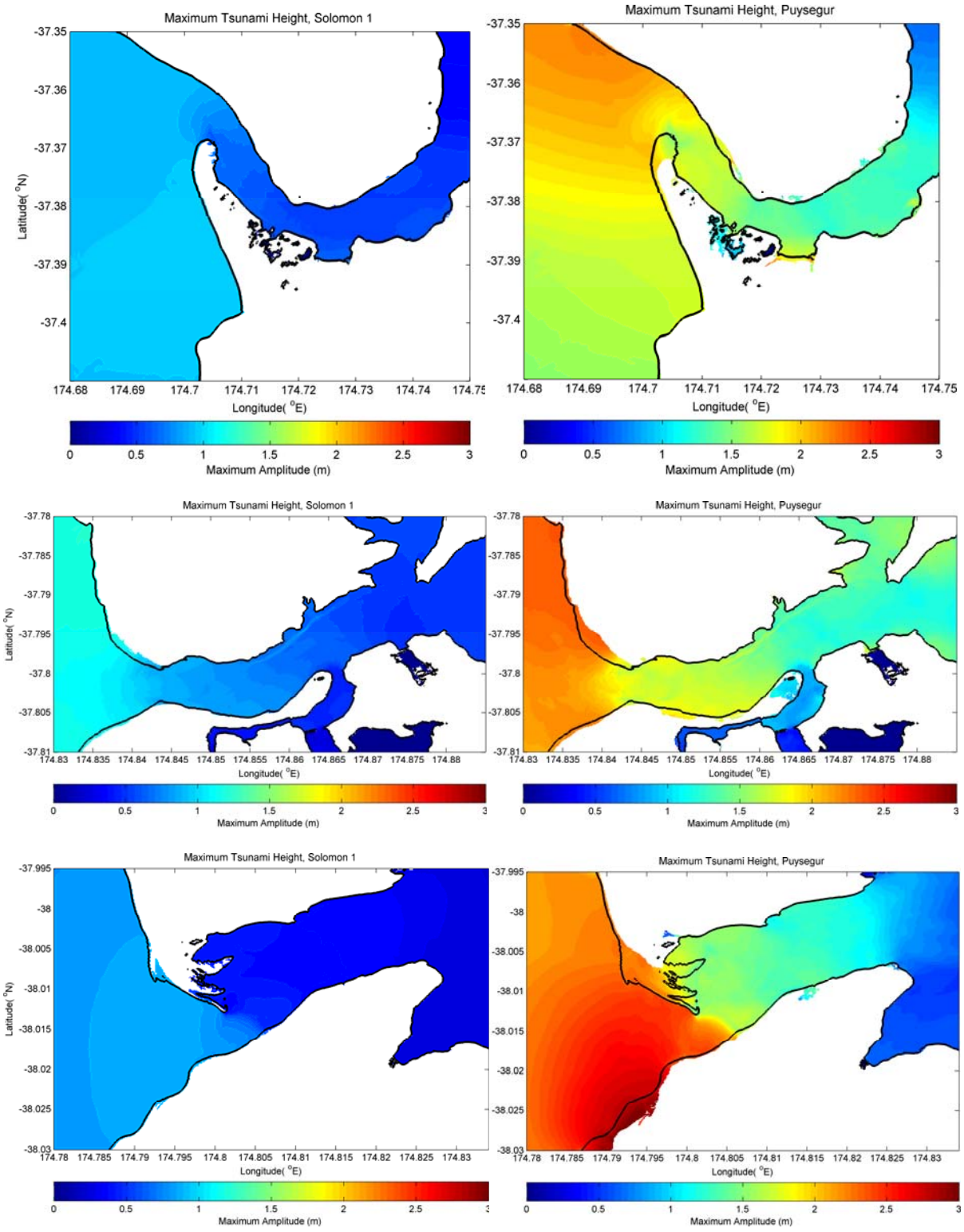

Figure 3.9 Maximum computed water levels for scenarios Solomon 1 (left) and Puysegur (right) at Aotea, Port Waikato and Raglan (top to bottom respectively); each case run at high tide.

AOTEA HARBOUR

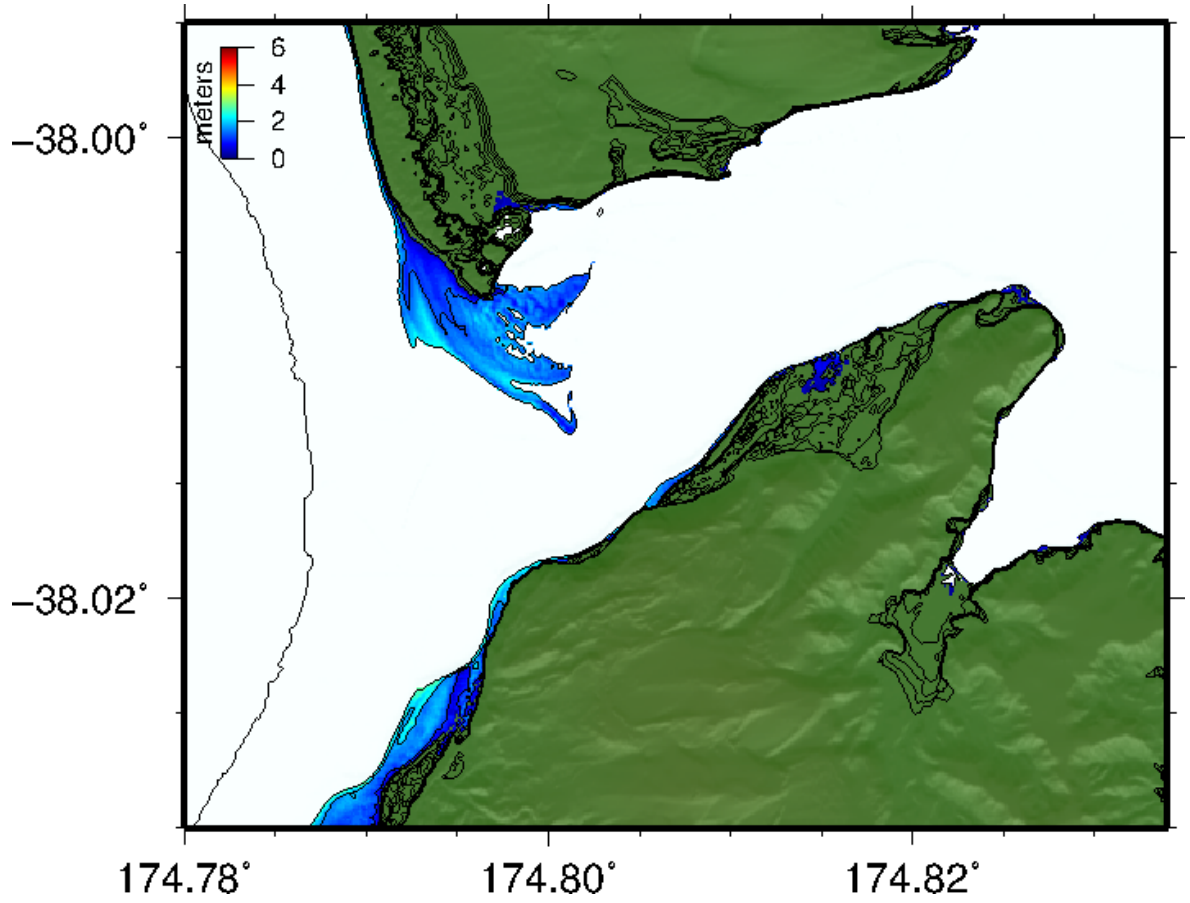

RAGLAN HARBOUR

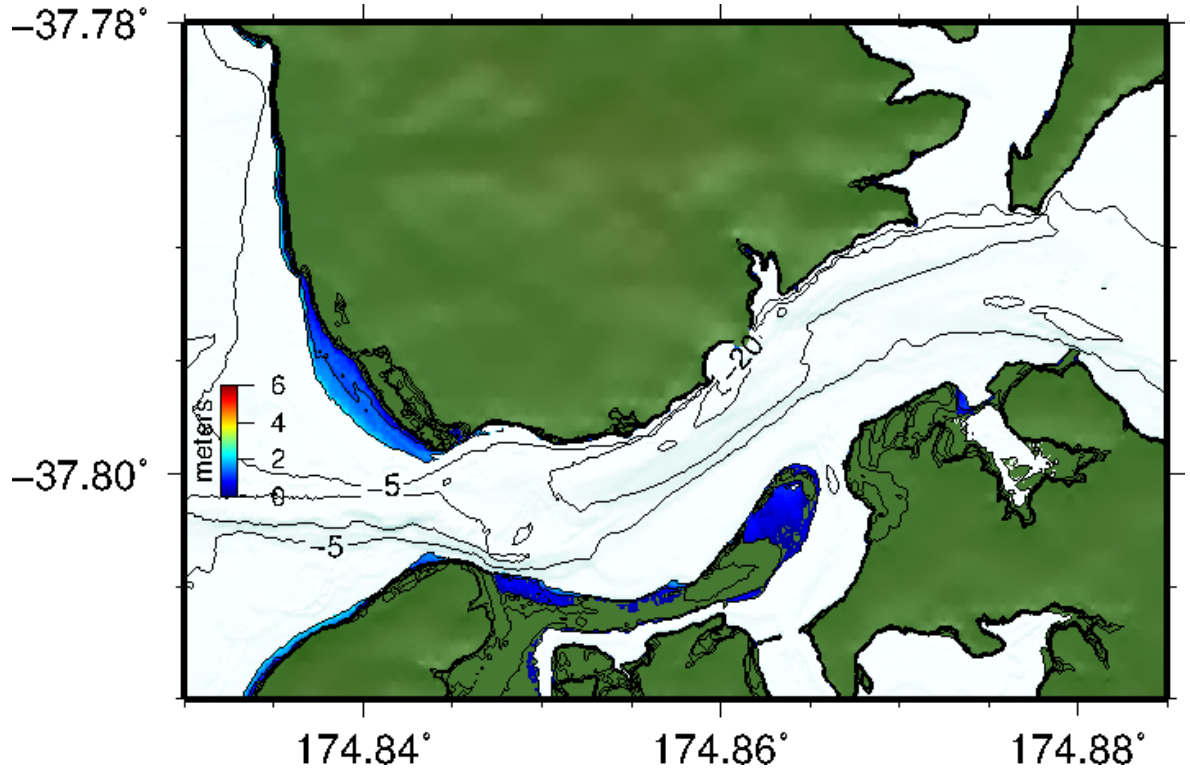

PORT WAIKATO

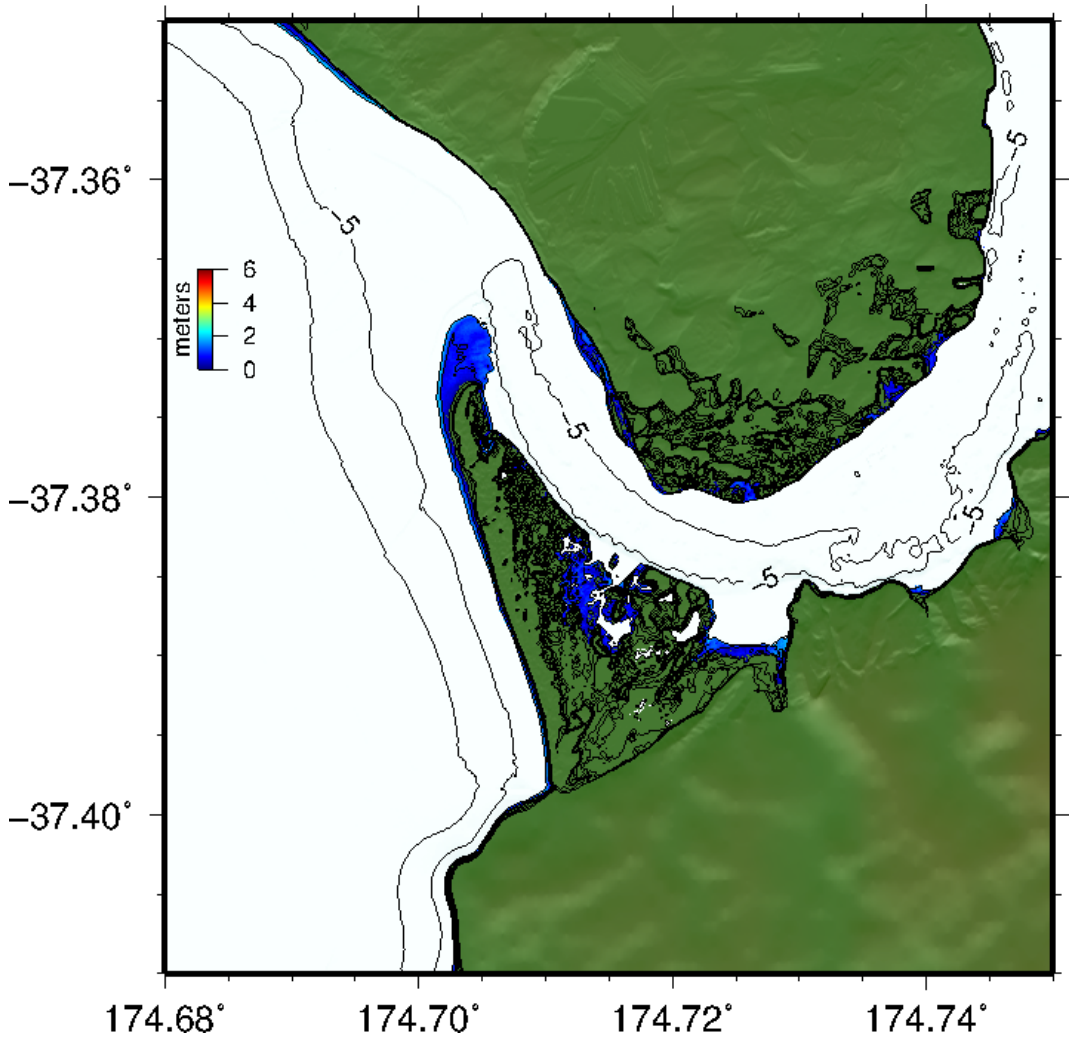

Figure 3.10 Flow depth plots for areas inundated by the Puysegur scenario at high tide at Aotea and Raglan Harbours (previous page) and Port Waikato (above).

3.3 Tsunami Current Speeds

Given the narrow entrances to Port Waikato, Raglan and Aotea Harbours, large current speeds are to be expected for some of the modelled tsunami scenarios. The variations in current speeds at these locations between the least and most severe scenarios (Solomon 1 and Puysegur respectively) are shown in Figure 3.11.

Perhaps more important than simply knowing the maximum current speeds, is also knowing the potential duration of strong currents. This concept is illustrated in the time-current-threshold maps shown in Figure 3.12. In this figure, we choose a particular current speed threshold and plot, as a colour, the time (in hours) over which that threshold is exceeded.

We emphasize here that this does not mean currents of this threshold are exceeded continuously over the time span indicated, but rather that the particular current speed threshold is exceeded at least once in that time period. In Figure 3.12 we compare the time-current threshold results between the Solomon 1 and Puysegur cases. The plots suggest that the Solomon 1 source has the potential to produce strong currents for up to 16 hours after tsunami arrival, however, this occurs only over relatively small areas in the Aotea and Port Waikato runs with a somewhat larger area affected in the Raglan case. In the Puysegur results however, we see that while the 3 knot threshold is exceeded over a larger portion of the harbour entrances, the duration generally lasts less than 12 hours. In the case of the Solomon 1 scenario, inspection of the water level time series plots above show a late arriving large surge that is likely the cause of the strong current late in the time series. Looking at the water level time series for the Puysegur case we see that the strongest tsunami effects occur between 3 and 9 hours after the earthquake. The full set of time-current-threshold maps is contained in the various appendices..

Current hazard plots are presented in Figure 3.13 through Figure 3.15. In these figures we plot the maximum computed current speeds for each source scenario using a banded colour palette. Presented this way, we can see which regions of the model domain are susceptible to what level of currents. The complete set of current hazard zone plots are presented for the three sites in the appendices.

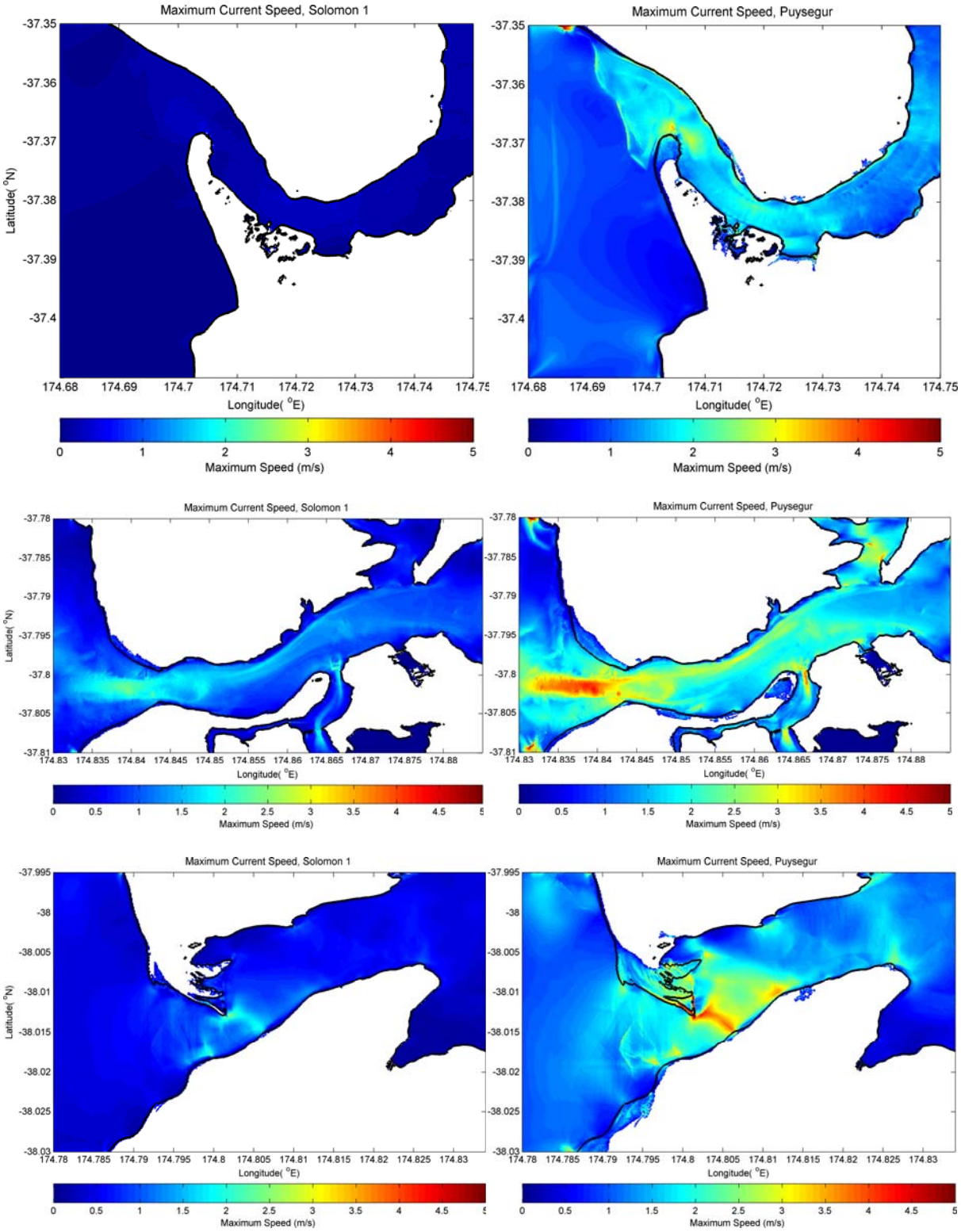

Figure 3.11 Computed maximum current speeds for scenarios Solomon 1 (left) and Puysegur (right) at Aotea, Port Waikato and Raglan (top to bottom respectively); each case run at high tide.

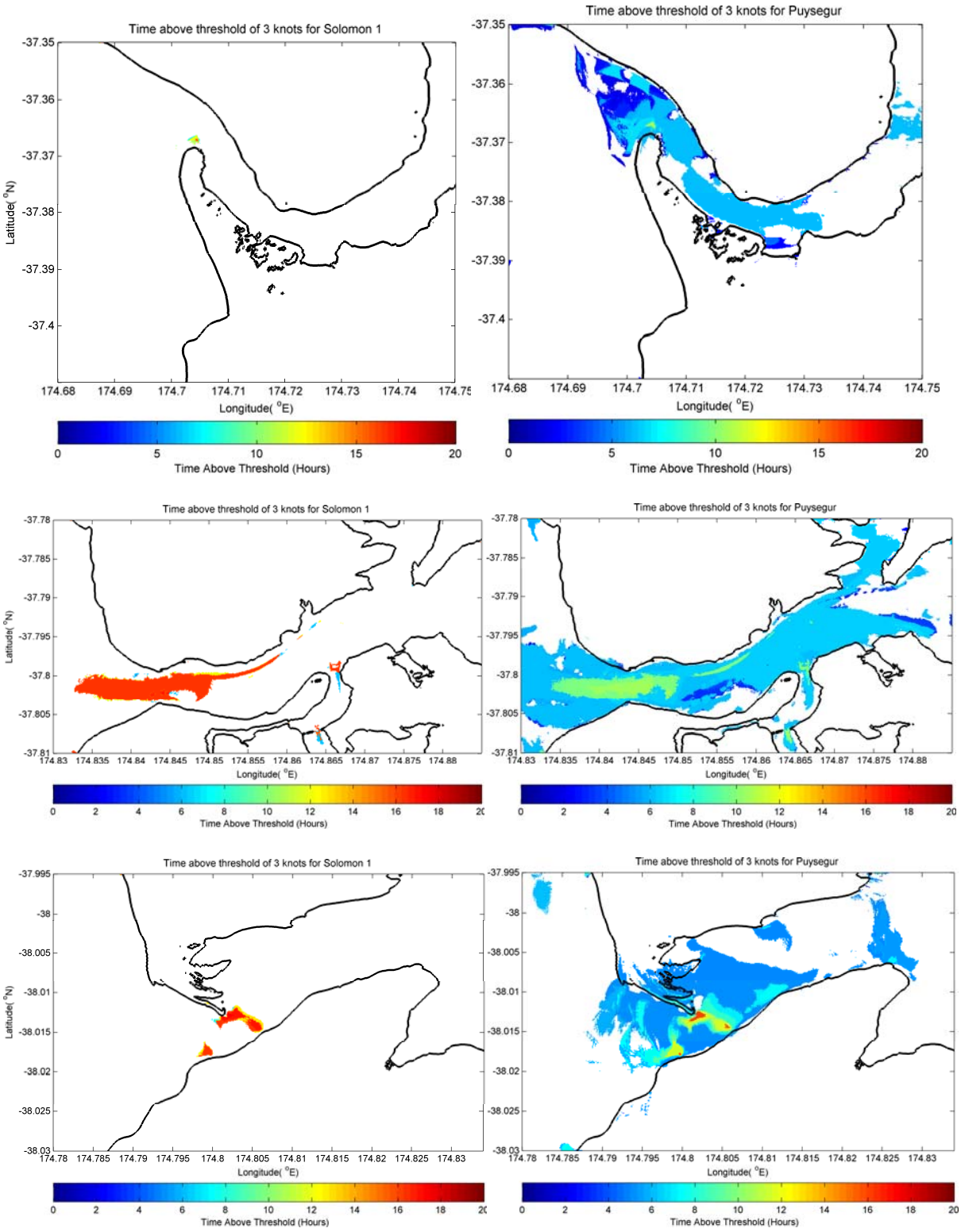

Figure 3.12 Time-current-threshold maps for scenarios Solomon 1 (left) and Puysegur (right) at high tide.

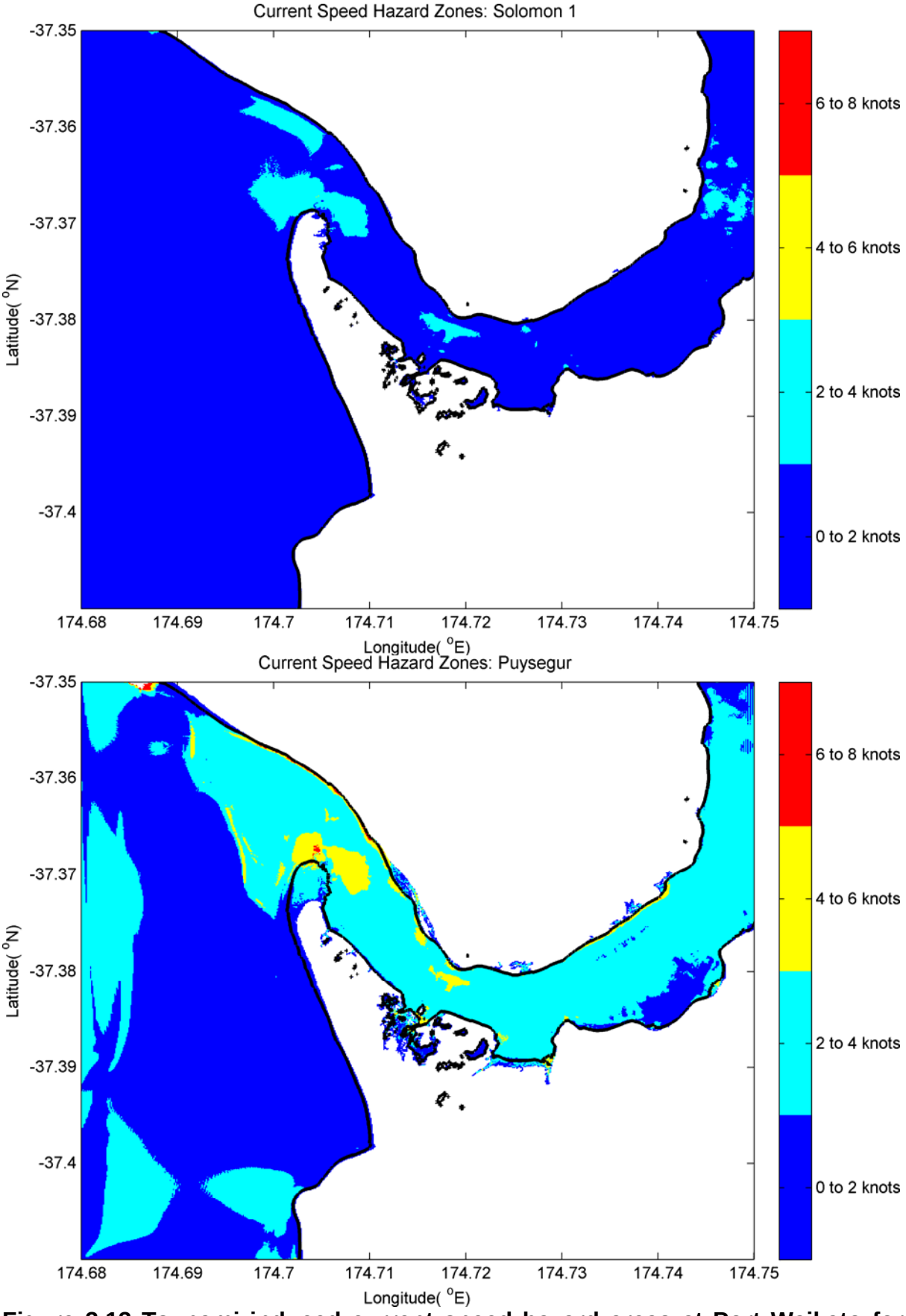

Figure 3.13 Tsunami induced current speed hazard areas at Port Waikato for the Solomon 1 (top) and Puysegur (bottom) tsunami sources.

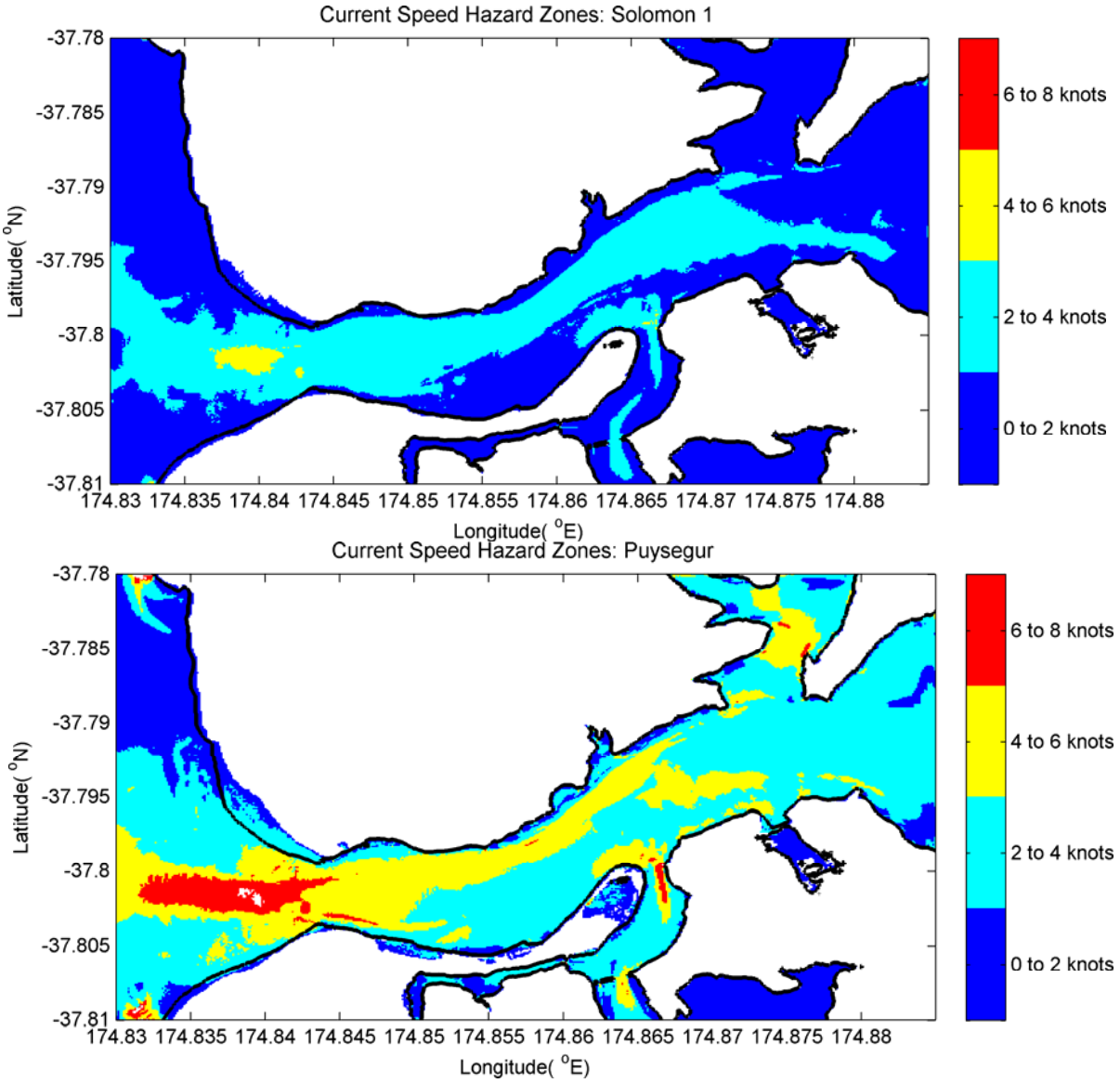

Figure 3.14 Tsunami induced current speed hazard areas at Raglan Harbour for the Solomon 1 (top) and Puysegur (bottom) tsunami sources.

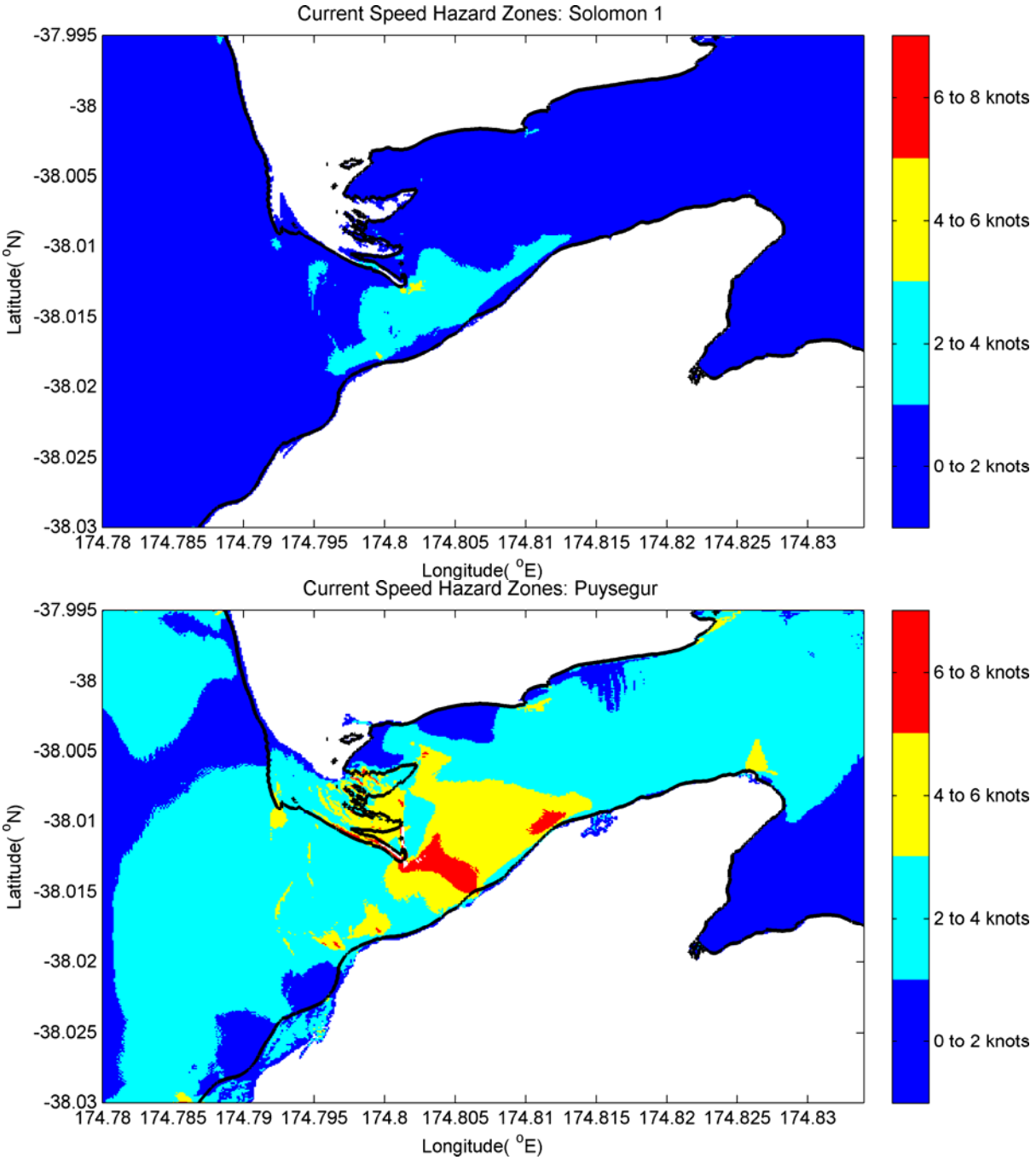

Figure 3.15 Tsunami induced current speed hazard areas at Aotea Harbour for the Solomon 1 (top) and Puysegur (bottom) tsunami sources.

4 MODEL RESULTS: DISTANT SOURCE TSUNAMIS

It is generally accepted that tsunamis generated along the Pacific rim would cause the strongest effects in New Zealand along the east and north facing coasts. The west coast of New Zealand is somewhat protected from north Pacific tsunamis by the shallow island chain ridges running from the Solomon Islands to Fiji. These shallow areas and complex bathymetric features act to reduce and scatter the incident tsunami wave trains. This effect is shown in Figure 4.1 for four large tsunamis (M9 earthquake source) emanating from the north Pacific region. However, the wave guide effect of the Lord Howe Rise and the Norfolk and Three Kings Ridges (see Figure 1.2) will still cause tsunami wave focussing and can lead to locally higher wave heights in some areas, yet we see in Figure 4.2 for the north Pacific case, the offshore tsunami heights are generally less than 1 m along the west coast of the North Island. For this reason, we focus our attention on tsunamis generated along the west coast of South America.

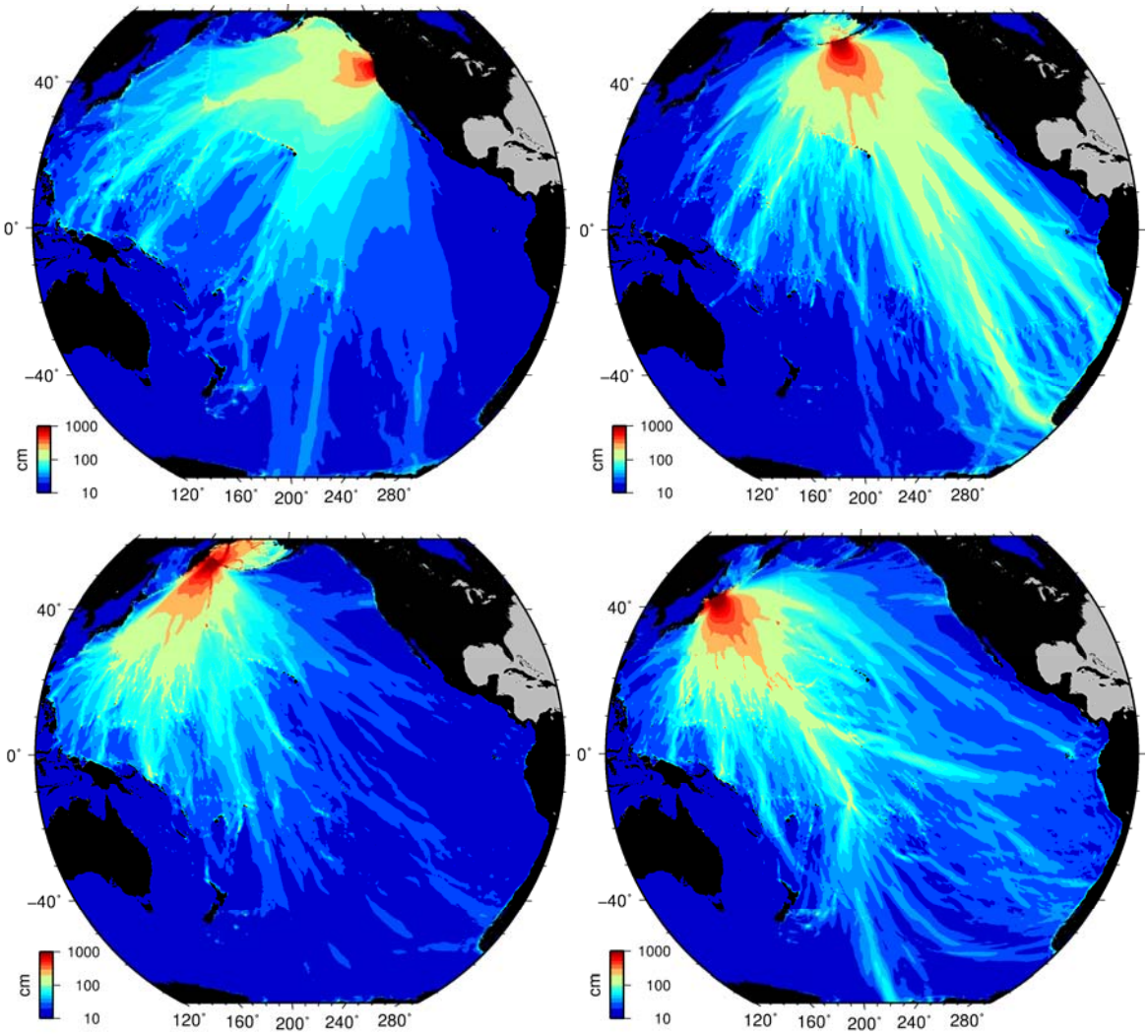

Figure 4.1 Modelled trans-Pacific tsunami wave heights for tsunami emanationg from the north Pacific.

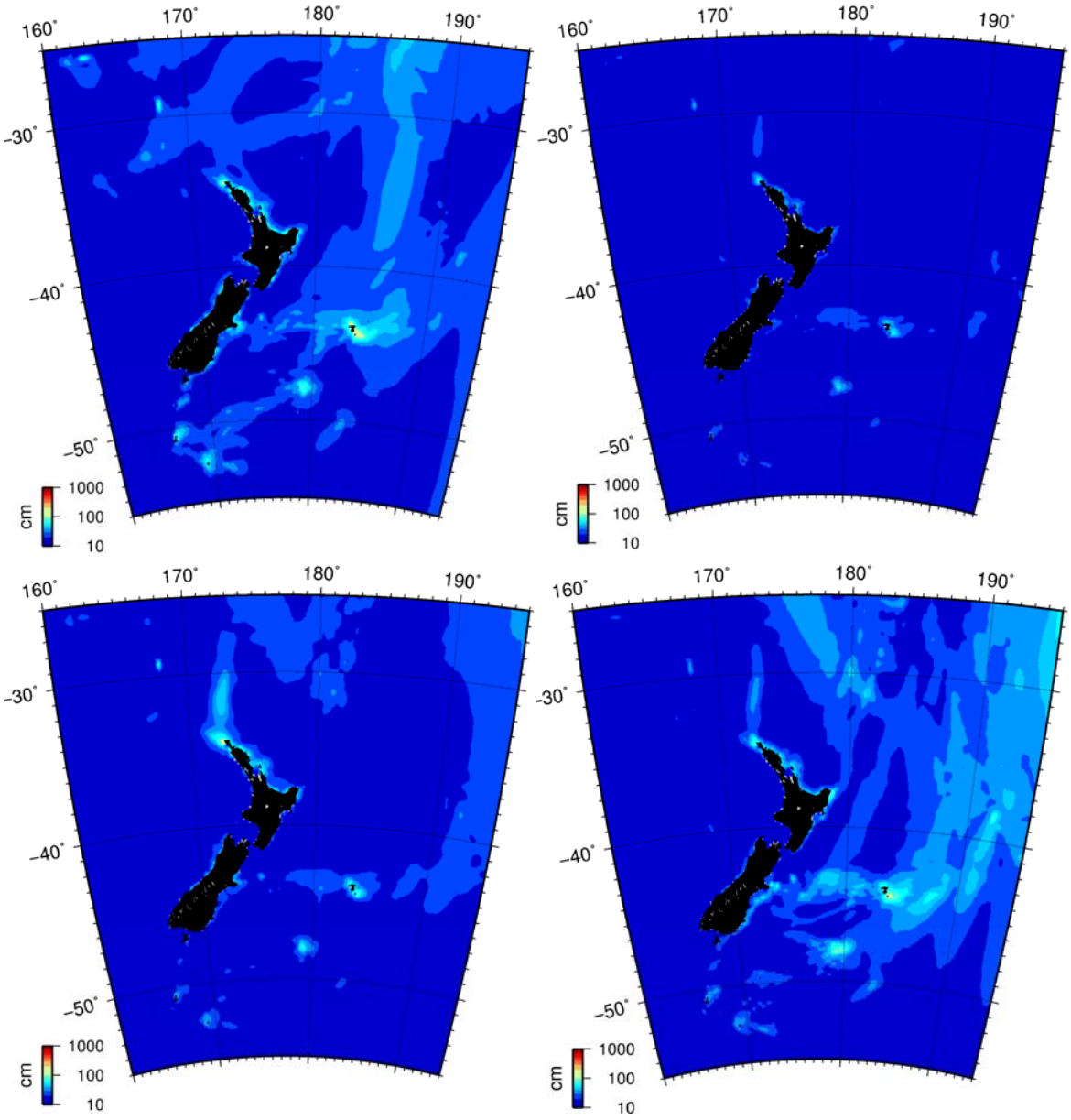

Figure 4.2 New Zealand regional tsunami wave heights from the four north pacific tsunami scenarios depicted in Figure 4.1.

4.1 Propagation Models

For tsunami sources along the west coast of South America, the strongest impact in New Zealand are again along the east coast of the North and South Islands. However, as seen in Figure 4.3, the west coasts are significantly sheltered from the tsunami waves. Thus, for this assessment, we conducted detailed modelling for the two largest tsunami sources available in the historic record, namely the 1960 Valdivia earthquake in southern Chile and the 1868 Arica earthquake that occurred in southern Peru and Northern Chile.

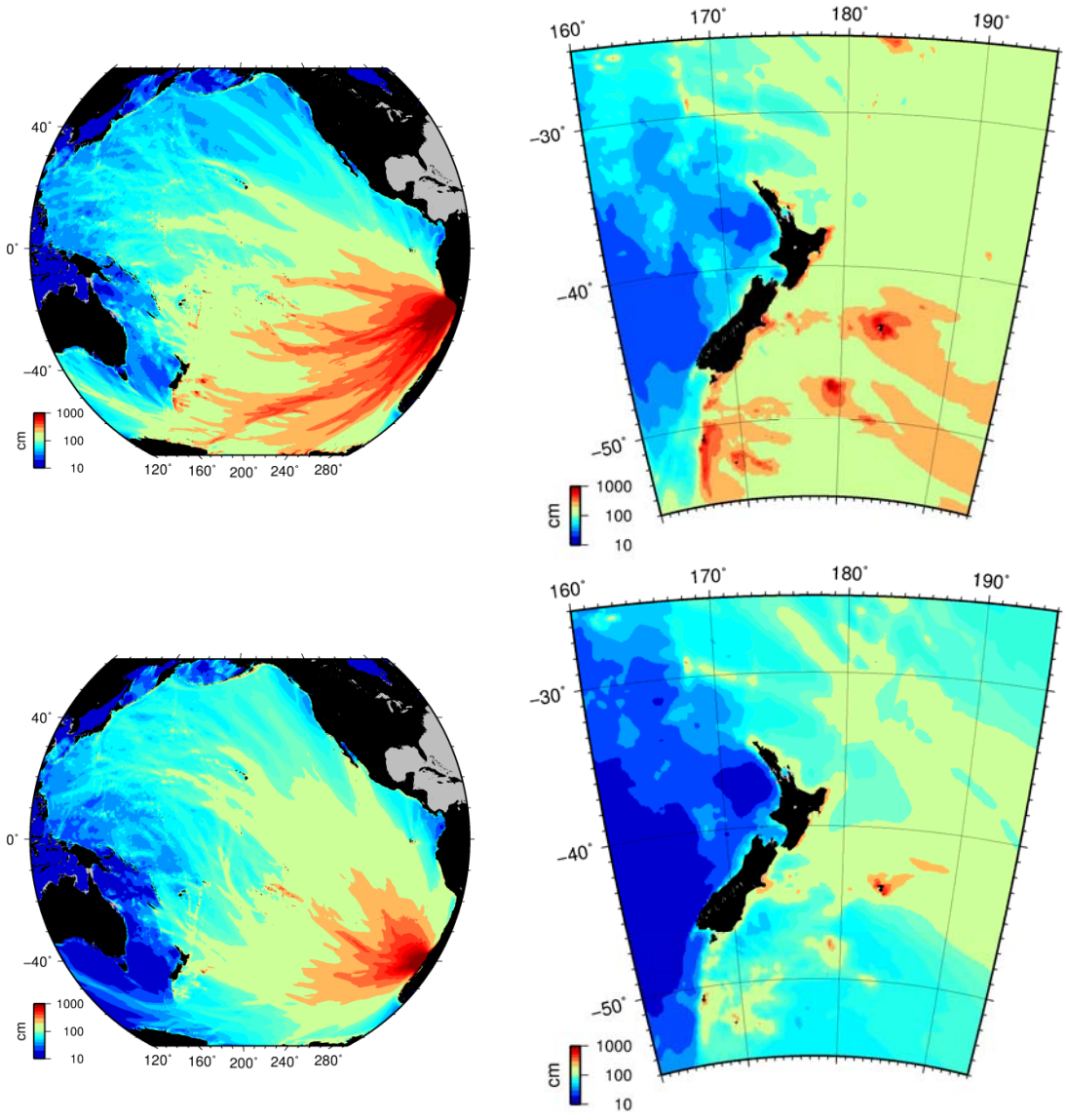

Figure 4.3 Trans-pacific and regional propagation plots for the 1868 Arica (top) and 1960 Valdivia tsunamis from Chile.

4.2 Arrival Times and Tsunami Heights

Modelled time series of water level at the entrance to and inside of Port Waikato, Raglan and Aotea Harbours for each of the far-field cases are presented in Figure 4.6 through Figure 4.6. We note that the 1960 southern Chile event arrives somewhat earlier than the 1868 Arica event, however it is also important to note that at each location, the largest surge occurs between many hours after tsunami arrival.

Tsunami heights are generally leas than 50 cm and do not cause any substantial inundation. This is consistent with the historical record which does not report any significant tsunami effects along the New Zealand west coast for far-field Pacific basin tsunamis.

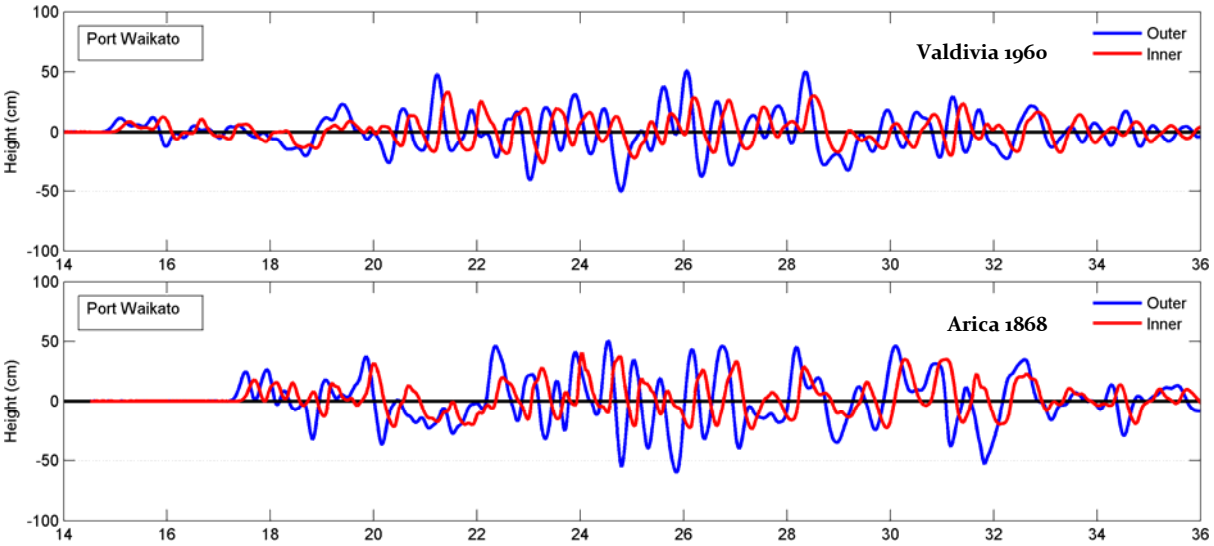

Figure 4.4 Water level time series for the 1960 (top) and 1868 (bottom) tsunamis at Port Waikato.

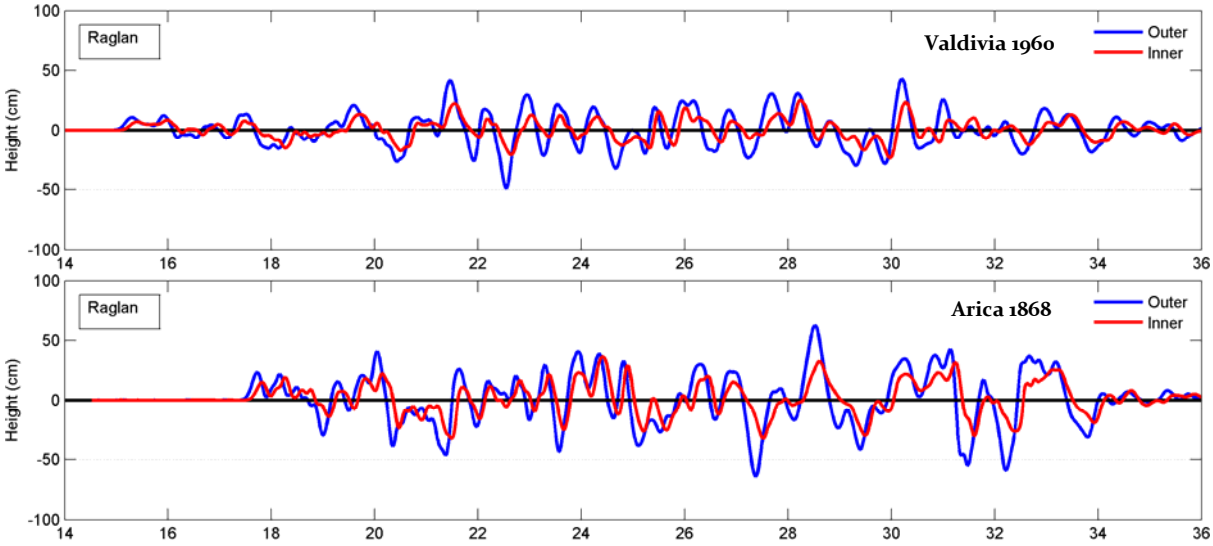

Figure 4.5 Water level time series for the 1960 (top) and 1868 (bottom) tsunamis at Raglan Harbour.

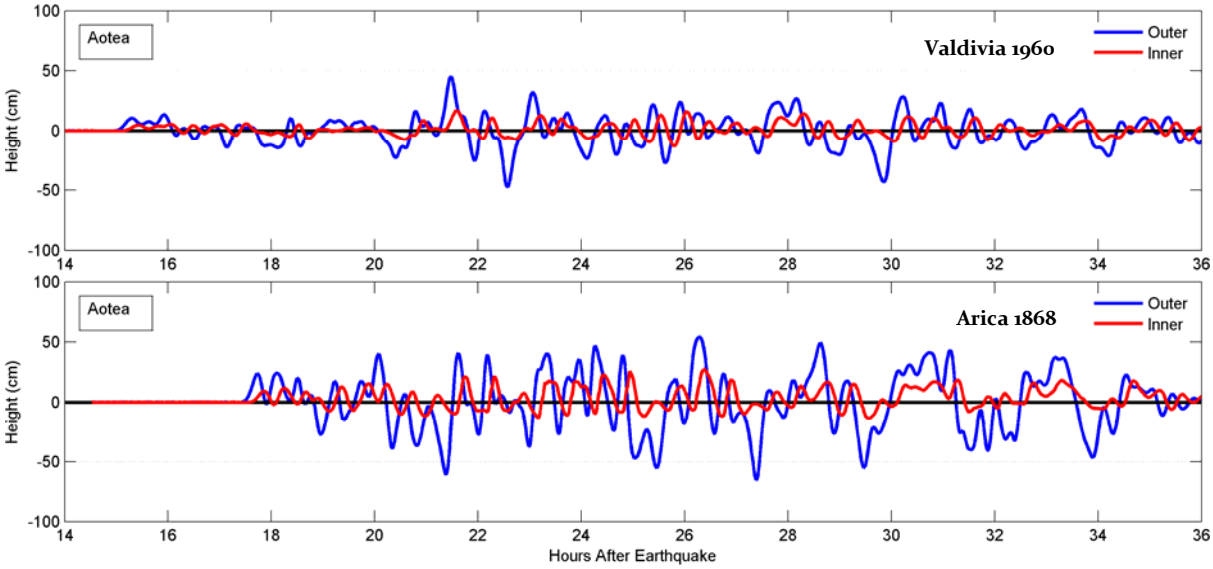

Figure 4.6 Water level time series for the 1960 (top) and 1868 (bottom) tsunamis at Aotea.

4.3 Tsunami Current Speeds

Consistent with the relatively small wave heights, the far field sources also produce overall low current speeds. Modelled maximum current speeds are generally less than 1.5 m/s (3 knots). Time-speed threshold plots show however that these currents speeds can persist for up to 20 hours after tsunami arrival (Figure 4.7).

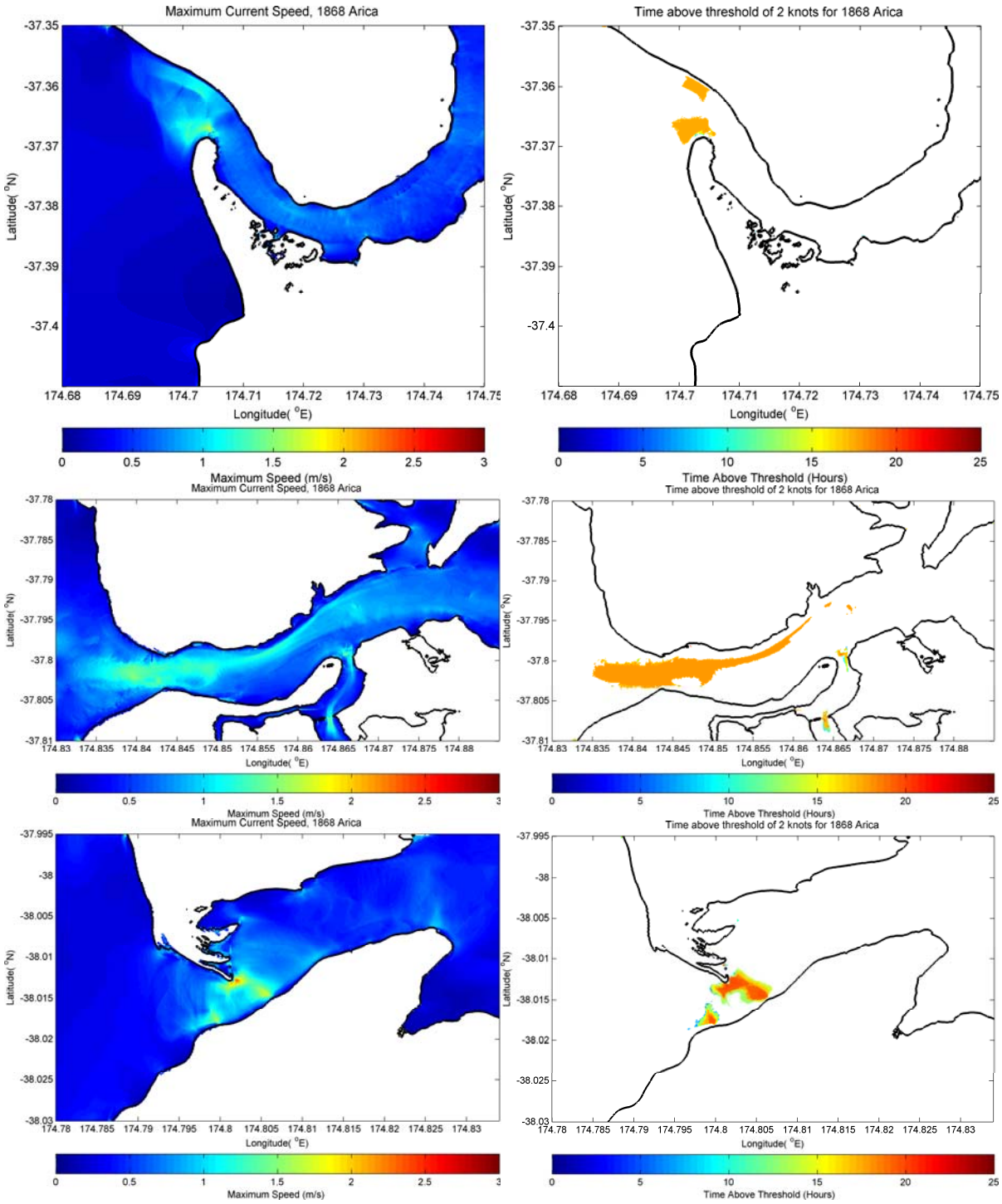

Figure 4.7 Maximum modelled current speeds and time-speed threshold plots for the 1868 Arica tsunami at the three study locations.

5 MODELLEING PREHISTORIC WEST COAST TSUNAMIS

Focussing on the enigmatic west coast tsunami of 1320-1450 AD hypothesized by Goff and Chagué-Goff (2015), we use a numerical modelling approach to investigate the tsunami propagation patterns of a landslide-type source occurring on or around the location of the Aotea Seamount. Although we do not rigorously simulate the dynamic formation of a landslide induced wave, we do model an initial condition that is reminiscent of a large landslide generated wave in terms of scale, i.e. 10's km rather than the 100's of km typical of a tectonic tsunami source. Furthermore, our tsunami source is of a dipole shape characteristic of landslide induced water waves.

For the modelling presented here we produced a static displacement of the water surface with an initial positive displacement of ~7 m and a negative displacement of ~4 m. The initial wave shape is positioned proximal to the Aotea seamount with the positive water surface deformation positioned towards shore representative of a translational slide or rotational slump moving down slope. We trialled three different slide orientations (striking 105˚, 120˚ and 135˚ along the long axis) to assess the sensitivity of the model results and determine areas of possible coastal focussing and defocussing of wave heights.

The results presents in Figure 5.1 show that for a given initial wave height of the scale of the Aotea Seamount, the initial wave heights are significantly reduced between the source and the coastline. For initial wave heights of ~11 m (+7 and -4), the wave heights at the coast are generally less than 1 m in height. This is likely the result of the relatively shallow bathymetry and the highly dispersive nature of the short, steep initial wave condition. There is some evidence of wave focussing producing larger wave heights in the southern corner of the Taranaki Bight, but there is no evidence of the extreme wave focussing needed to produce the 60 m runup heights at Ngararahae as hypothesized by Goff and Chagué-Goff (2015). In Figure 5.2 we show the effect of doubling the height of the dipole initial condition (~22 m height range, +14 m to -8 m). While this produces noticeably larger wave heights at the coast, it is still insufficient to produce the 30 to 60 m heights discussed by Goff and Chagué-Goff (2015).

For illustrative purposes, in Figure 5.2 we also show the effect of a longer, wider source model, representative of an earthquake-type dislocation centred on the Aotea Seamount. It is apparent that the longer source produces more concentrated and larger wave heights along the shoreline. However, this type of earthquake source does not exist in the Tasman Sea.

Ultimately, it is very difficult to reconcile the geologic evidence presented by Goff and Chagué-Goff (2015) suggestive of 30 to 60 m tsunami runup heights along the coast of south west Waikato with numerical modelling of potential tsunami source whether they be regional or near field.

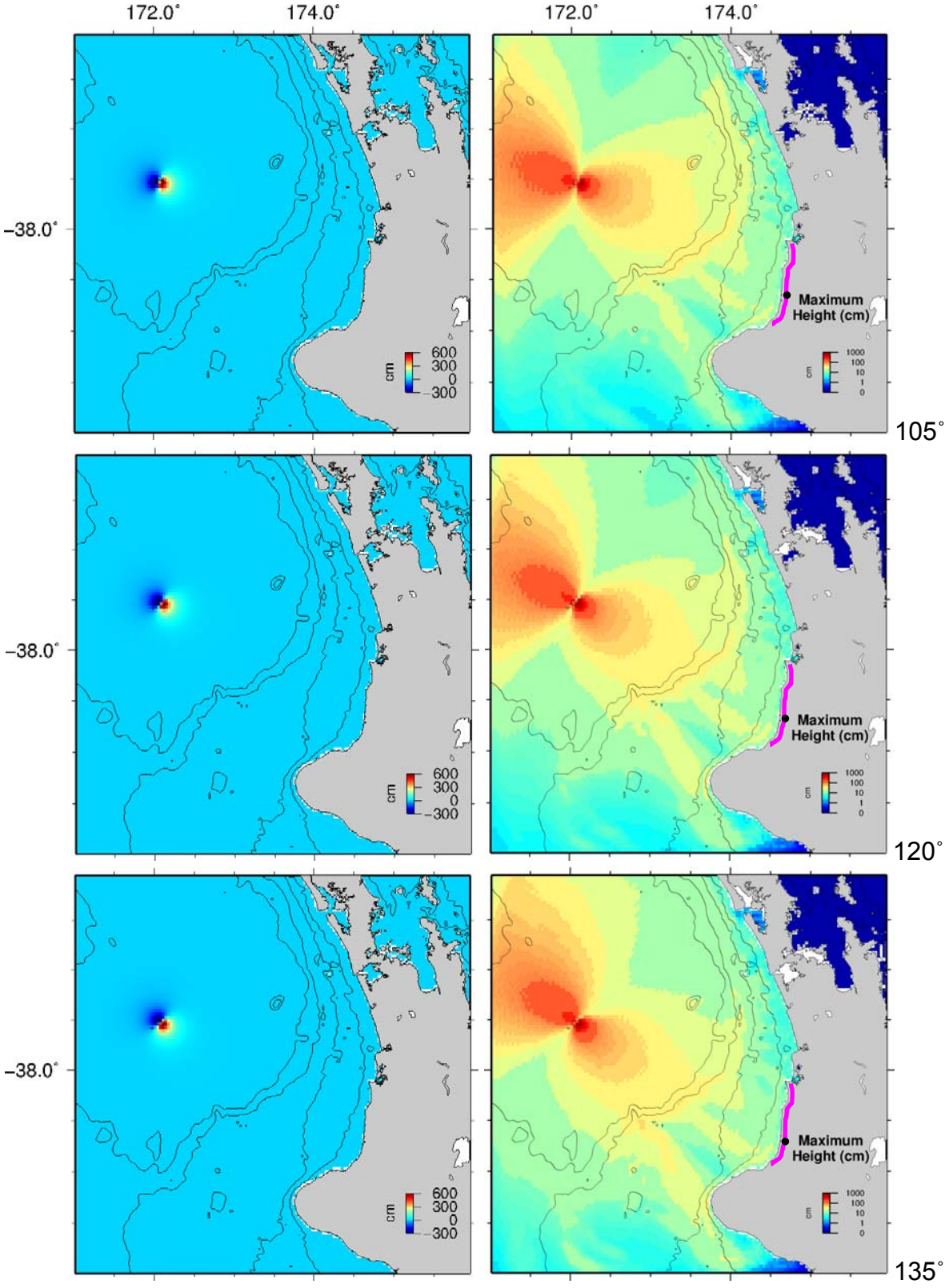

Figure 5.1 Initial surface displacements and maximum modelled wave heights (log scale) for hypotehtical tsunami sources on the Aotea Sea Mount for three different source orientations. The section of coast highlighted in magenta is the region where Goff and Chagué-Goff (2015) have estimated runup heights of 30 m or greater. The Black dot is Ngarahae, location of 60 m estimated runup

heights.

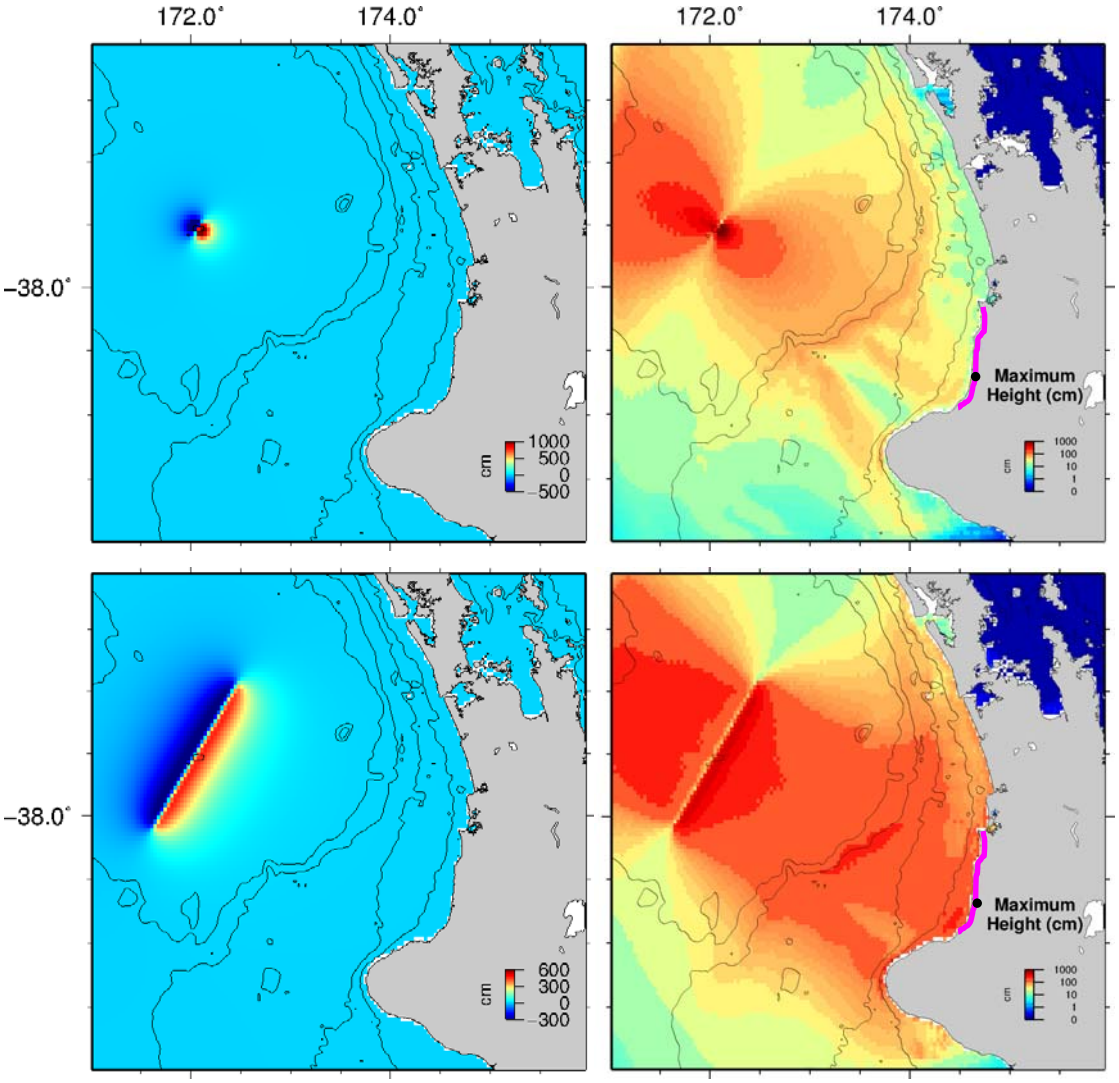

Figure 5.2 Comparing results for a dipole source with twice the inintial wave height (top) and a long source (representative of an earthquake rupture).

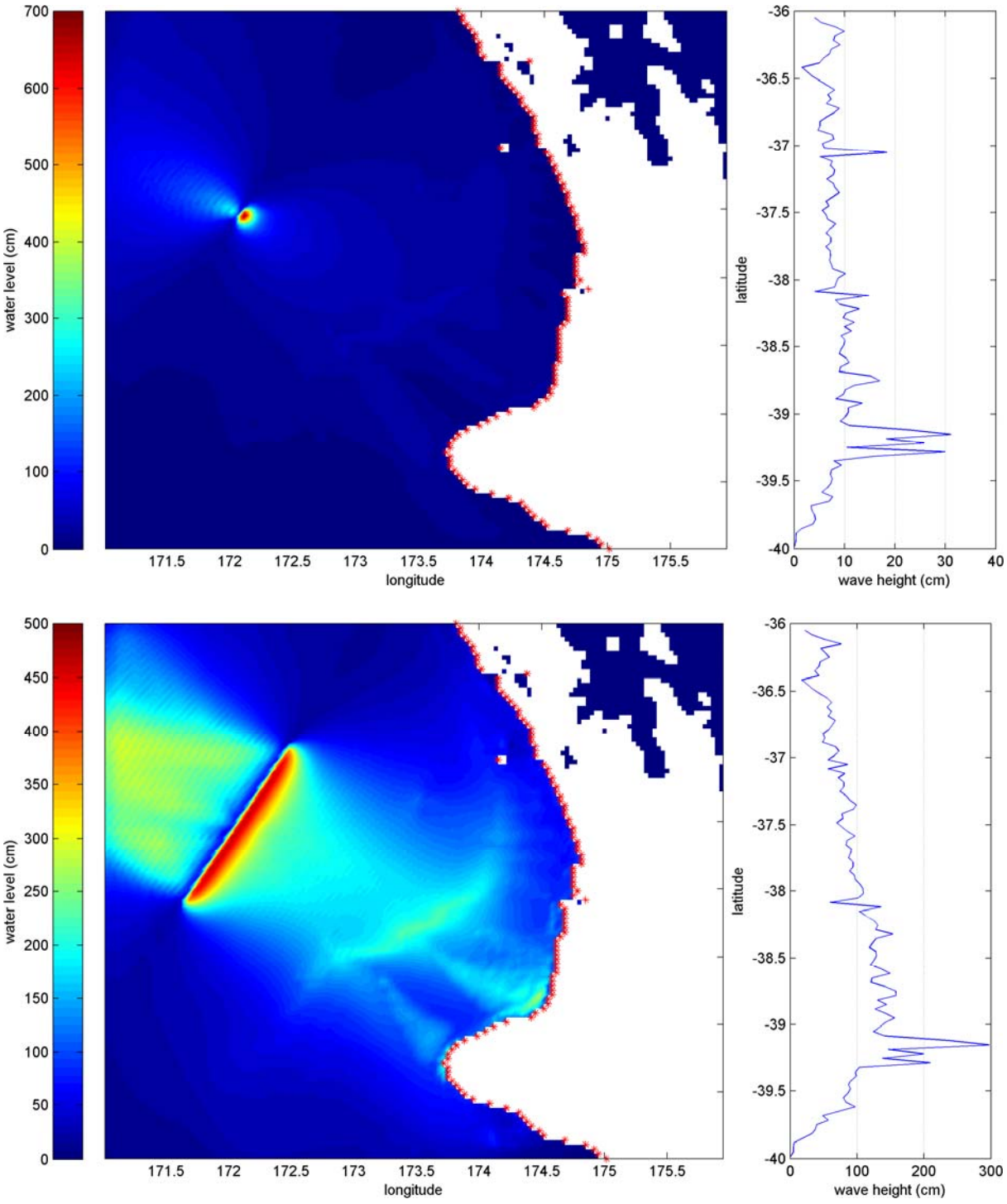

Figure 5.3 Comparison of along shore unup heights from a dipole source (top) and a longer, wider source (bottom). Note the different scales on the runup plots to the right.

6 SUMMARY AND CONCLUSIONS

We have evaluated the tsunami hazards at three locations on the west coast of North Island New Zealand; Port Waikato, Raglan Harbour and Aotea Harbour for several regional and far-field tsunami sources. The assessment includes maximum tsunami wave heights, tsunami inundation and tsunami induced current speeds. We also assessed nearshore tsunami heights along the west coast as a result of possible near field landslide or slump sources. These model results will be used by the Waikato Regional Council and the Waikato District Council as part of evacuation planning and emergency management activities as well as for education and outreach activities amongst the potentially affected populations.

For the regional sources we focus on the Southern New Hebrides, Solomon, Puysegur and Tonga-Kermadec Trenches, and consider a large magnitude (M9.0) events located along each subduction zone plate boundary. Source models were based on interpolate subduction earthquakes with a fault plane of 400 km x 100 km and uniformly distributed slip of 22 m. Of the cases modelled, only the Puysegur event produces significant wave heights at the study sites and are seen to be in the order of 2 to 2.5 m. All scenarios however produce potentially dangerous tsunami currents, particularly at the entrance to each harbour, and persist for many hours after the arrival of the largest wave. The arrival times from these regional sources is relatively short, approximately 3 – 5.5 hours for the initial withdrawal of the water surface with the first tsunami peak arriving some 15 to 30 minutes afterwards. In most cases at all three harbours, the first wave was not the largest of the tsunami wave train. The exception was this was for the TK 1 scenario which produced the first arriving wave as the largest. Furthermore, for these sites, the overall characteristics of the tsunami wave train were much more varied and complex with surges of significant height persisting for many hours after tsunami arrival.

For the far-field sources, we consider two large magnitude earthquake sources along the South American subduction zone representing the 1868 Arica and 1960 Valdivia, historical Chilean events. Neither of these scenarios produce significant tsunami wave heights at Port Waikato, Raglan or Aotea. For both of these modelled cases, the peak tsunami wave height occurred more than 6.5 and as much as 11 hours after tsunami arrival. This is an important consideration for tsunami warnings for large, far-field events. In terms of tsunami induced current speeds, the far-field sources produce lower peak current speeds than the regional sources, however, the duration of the currents is much longer, with current speeds of more than 2 knots persisting for up to 16 hours after tsunami arrival.

Finally, we conducted a preliminary numerical modelling investigation in to the source of the very large (30 – 60 m) tsunami runup heights along the western Waikato coast as hypothesized by Goff and Chagué-Goff (2015). The results suggest that if the causative mechanism were a slump on the Aotea Seamount, initial water surface displacements would need to be of the order of 100 m to produce runup heights anywhere near the 30 m (let alone 60 m!) heights required. However, sources with larger dimensions (i.e. longer and wider) produce proportionally larger nearshore tsunami heights as compared to the short, steep wave heights produced from

submarine slumps or landslides. If the findings of Goff and Chagué-Goff (2105) are to be believed, then the possible source for such a wave remains a mystery.

7 REFERENCES

Borrero, J. C. (2013). *Numerical modelling of tsunami effects at two sites on the Coromandel Peninsula, New Zealand: Whitianga and Tairua-Pauanui* (No. 2013/24) (Vol. 4355, pp. 1–96).

Borrero, J. C. (2014). *Numerical modelling of tsunami effects at Whangamata, Whiritoa and Onemana, Coromandel Peninsula New Zealand*, Report prepared for the Waikato Regional Council, September 2014.

Borrero J.C. and Goring D.G (2015) South American Tsunamis in Lyttelton Harbor, New Zealand, *Pure and Applied Geophysics*, Volume 172, Issue 3, pp 757-772.

Borrero, J.C., Goring, D.G., Greer, S.D. and Power, W.L. (in review) Far-Field Tsunami Hazard in New Zealand Ports, *Pure and Applied Geophysics*, Volume 172, Issue 3, pp 731-756 .

De Lange, W. P., & Haley, T. R. (1986). New Zealand tsunamis 1840–1982. *New Zealand Journal of Geology and Geophysics*, *29*(1), 115–134. doi:10.1080/00288306.1986.10427527

Fujii, Y., & Satake, K. (2012). Slip Distribution and Seismic Moment of the 2010 and 1960 Chilean Earthquakes Inferred from Tsunami Waveforms and Coastal Geodetic Data. *Pure and Applied Geophysics*, *170*(9-10), 1493–1509. doi:10.1007/s00024-012-0524-2

Goff, J., and Chagué-Goff, C. (2014). The Australian tsunami database: A review *Progress in Physical Geography* 201438:218 DOI:10.1177/0309133314522282.

Goff, J., and Chagué-Goff, C. (2015). Three Large Tsunamis on the Non-Subduction, Western Side of New Zealand over the past 700 years. *Marine Geology, 363*(2015), 243-260.

Power, W. L., & Gale, N. (2010). Tsunami Forecasting and Monitoring in New Zealand. *Pure and Applied Geophysics*, *168* (6-7), 1125–1136. doi:10.1007/s00024-010-0223-9

Power, W. L., Downes, G., & Stirling, M. (2007). Estimation of Tsunami Hazard in New Zealand due to South American Earthquakes. *Pure and Applied Geophysics*, *164*(2-3), 547–564. doi:10.1007/s00024-006-0166-3

Power, W. L., Wallace, L., Wang, X., & Reyners, M. (2011). Tsunami Hazard Posed to New Zealand by the Kermadec and Southern New Hebrides Subduction Margins: An Assessment Based on Plate Boundary Kinematics, Interseismic Coupling, and Historical Seismicity. *Pure and Applied Geophysics*, *169*(1-2), 1–36. doi:10.1007/s00024-011-0299-x

Prasetya, G. S., & Wang, X. (2011). *Tsunami frequency analysis for Eastern Coromandel and Waikato Region from Kermadec Trench and local sources within the Bay of Plenty* (No. 2011/135) (p. 65).

Power, W. L. (compiler). 2013. Review of Tsunami Hazard in New Zealand (2013 Update), GNS Science Consultancy Report 2013/131. 222 p.

Titov, V. V., & González, Frank, I. (1997). *Implementation and testing of the Method of Splitting Tsunami (MOST) model* (No. ERL PMEL-112) (p. 14). Retrieved from http://www.pmel.noaa.gov/pubs/PDF/tito1927/tito1927.pdf

Titov, V. V., Moore, C. W., Greenslade, D. J. M., Pattiaratchi, C., Badal, R., Synolakis, C. E., & Kânoğlu, U. (2011). A New Tool for Inundation Modeling: Community Modeling Interface for Tsunamis (ComMIT). *Pure and Applied Geophysics*, *168*(11), 2121–2131. doi:10.1007/s00024-011-0292-4

Titov, V.V., and C.E. Synolakis (1995): Modeling of breaking and nonbreaking long wave evolution and runup using VTCS-2. J. Waterways, Ports, Coastal and Ocean Engineering, 121(6), 308–316.

Titov, V.V., and C.E. Synolakis (1997): Extreme inundation flows during the Hokkaido-Nansei-Oki tsunami. Geophys. Res. Lett, 24(11), 1315–1318.